Shock and Vibration 14 (2007) 181–228
IOS Press

Field tests and simulation of Lion-Head River Bridge

Yao-Min Fang[a] and Jun-Ping Pu[b]
[a]*Graduate Institute of Civil and Hydraulic Engineering, Feng Chia University, Taichung, Taiwan*
Tel.: +886 4 24517250 4549; Fax: +886 4 24516982; E-mail: ymfang@ms36.hinet.net
[b]*Department of Civil Engineering, Feng Chia University, Taichung, Taiwan*
Tel.: +886 4 24517250 3120; Fax: +886 4 24516982; E-mail: jppu@fcu.edu.tw

Received 13 June 2005
Revised 28 April 2006

Abstract. Lion-Head River Bridge is a twin bridge in parallel position. The east-bounded was designed and constructed as a traditional prestress concrete box girder bridge with pot bearings; and the west-bounded was installed with seismic isolation devices of lead rubber bearings. The behavior of the isolated bridge is compared with that of the traditional bridge through several field tests including the ambient vibration test, the force vibration test induced by shakers, the free vibration test induced by a push and fast release system, and the truck test. The bridges suffered from various extents of damage due to the Chi-Chi and the Chi-I earthquakes of great strength during the construction and had been retrofitted. The damage was reflected by the change of the bridges' natural frequencies obtained from the ambient vibration tests. The models of the two bridges are simulated by the finite element method based on the original design drawings. Soil-structure interaction was also scrutinized in this study. The simulation was then modified based on the results from the field tests. Dynamic parameters of bridges are identified and compared with those from theoretical simulation. The efficiency is also verified to be better for an isolated bridge.

Keywords: Bridge, lead rubber bearings, field test

1. Introduction

Field tests are important procedures for knowing the performance and dynamic properties including natural frequencies, modal shapes and damping ratios. These tests make it possible to compare with the actual behavior and simulation of a bridge subjected to various types of loading. These properties can be used to update the numerical models of the bridge, and reflect better for the in-situ boundary conditions.

An ambient vibration test does not have consider nor input of any excitation, which is extremely convenient, and does not require a long time to measure. The analysis is fast and can accurately respond to the main vibration frequencies of bridges.

C.S. Huang [1] determined the natural frequencies, modal damping ratios and modal shapes of a structure from the ambient vibration, free vibration and earthquake response data. The feasibility of the procedure is demonstrated through processing an in-situ ambient vibration measurement of a five-story steel frame, an impulse response measurement of a three-span continuous bridge, and simulated earthquake responses of five-story steel frames to shaking table tests. C.R. Farrar [2] used the cross-correlation function between two response measurements from an ambient excited structure, which is shown to have the same form as the system's impulse response function. The resonant frequencies of a highway bridge, that were identified by curve-fitting the cross-correlation functions using traffic excitation as the ambient vibration source, are compared to modal properties identified by standard forced vibration testing methods. This experimental verification implies that the proposed method of analyzing ambient vibration data can be used to accurately assess the dynamic properties of structures in a non-intrusive manner. Ayman A. Shama [3] applied an experimental ambient vibration field investigation with a companion computational

ISSN 1070-9622/07/$17.00 © 2007 – IOS Press and the authors. All rights reserved

modeling study of a cantilever truss bridge. The ambient vibration experiments were conducted on the central suspended span and two adjacent anchor spans of the North Grand Island (NGI) Bridge. In a three-dimensional finite element model, the bridge is validated against the experimental results. A nonlinear static procedure using the capacity–demand spectrum approach is then employed to evaluate the expected seismic performance of the structure.

As for the isolated bridges, Eric Abrahamson [4] models the behavior of seismic response modification devices developed for use in analyzing bridge structures. The lead-rubber bearing element has a nonlinear elastic longitudinal spring, and a biaxial kinematic hardening spring in the transverse plane. The formulation and verification of the elements are presented. Ruben L. Boroschek [5] deals with the mechanical and dynamic characteristics of a 383 m long seismic isolated bridge located in a high seismic risk area. The tests carried out on rubber components, isolators and the bridge structure are presented. A strong motion permanent network installed on the bridge allowed the recording of ambient-traffic vibrations as well as seismic motions. Seismic records show the beneficial effect of the isolation in the horizontal direction, but important amplification occurs in the vertical direction for relatively high frequency components. Qingbin Chen [6] used a simple procedure for identifying hysteretic properties of seismically isolated bridges from full-scale quick-release tests. An analytical solution for the quick-release response of a SDOF system with a bilinear spring is derived, based on the solution, and some characteristics of such systems are obtained. H. Kaplan [7] investigates the feasibility of developing an active base isolation system for the protection of bridges subjected to earthquakes. A hydraulic actuator was used to force it to rotate to the locking position under fluid pressure which would be constantly maintained at the design level during normal conditions. The actuator was equipped with a quick response release valve for rapidly releasing the pressure and consequently unlocking the cam as soon as an earthquake is detected. J.S. Hwang [8] based on a previous application of the fractional derivative Kelvin model to the seismic response prediction of high damping rubber (HDR) bearings. The effect of ambient temperature is incorporated with the formulation of the model, considering that the variation of ambient temperature may significantly influence the mechanical characteristics of the bearings. Shaking-table tests are conducted for a test structure composed of a steel deck isolated by four HDR bearings. The extended model is validated by comparing the predicted seismic responses of the test structure with those measured from the earthquake tests conducted at various temperatures.

L. Fryba [9] describes the static, dynamic and long-term tests of bridges in-situ, which have been performed in the Czech and Slovak Republics since 1968. The monitoring of stresses under usual traffic loads provides important data for the fatigue of bridges, for the estimation of their residual life-spans and for the determination of inspection frequencies. Modal analysis and identification ascertain the characteristic properties of bridges from their response. The damage in bridges may be detected by the changes of their natural frequencies or modes of natural vibration.

Because of the development and the advantage of an isolated bridge, The Taiwan Area National Expressway Engineering Bureau, Ministry of Transportation and Communication chose the Lion-Head River Bridge, located in a high seismic risk area, to be designed as parallel twin bridges, with the east-bounded and west-bounded as a traditional and an isolated bridge respectively for comparison purposes.

During the construction period, the bridges are subjected to the Chi-Chi (September 21) earthquake and the Chia-I (October 22) earthquake in 1999. Several bearings were damaged. The bridges were hence retrofitted afterward.

This paper examined and compared the behaviors of conventional and isolated bridges under several types of dynamic tests. A series of dynamic tests, including the ambient vibration test, the free vibration test, the forced vibration test and the truck test, were conducted. Different characteristics of these two bridges were observed. The dynamic parameters of bridges are identified and compared with those from theoretical simulation. The efficiency of an isolated bridge was analyzed.

2. The profile of Lion-Head River Bridge

The Lion-Head River Bridge is located in Chi-I County, Taiwan. The site is considered a hard soil area, based on the information from geological drilling. The standard penetration tests show that the N values are all larger than 100.

The total length of the bridge is about 170 m. The superstructure of each bridge is a continuous box girder with five spans. There is a 20 cm-width gap between the decks of the east-bounded and the west-bounded bridges. The cross-section and elevation view of the bridges are shown in Fig. 1.

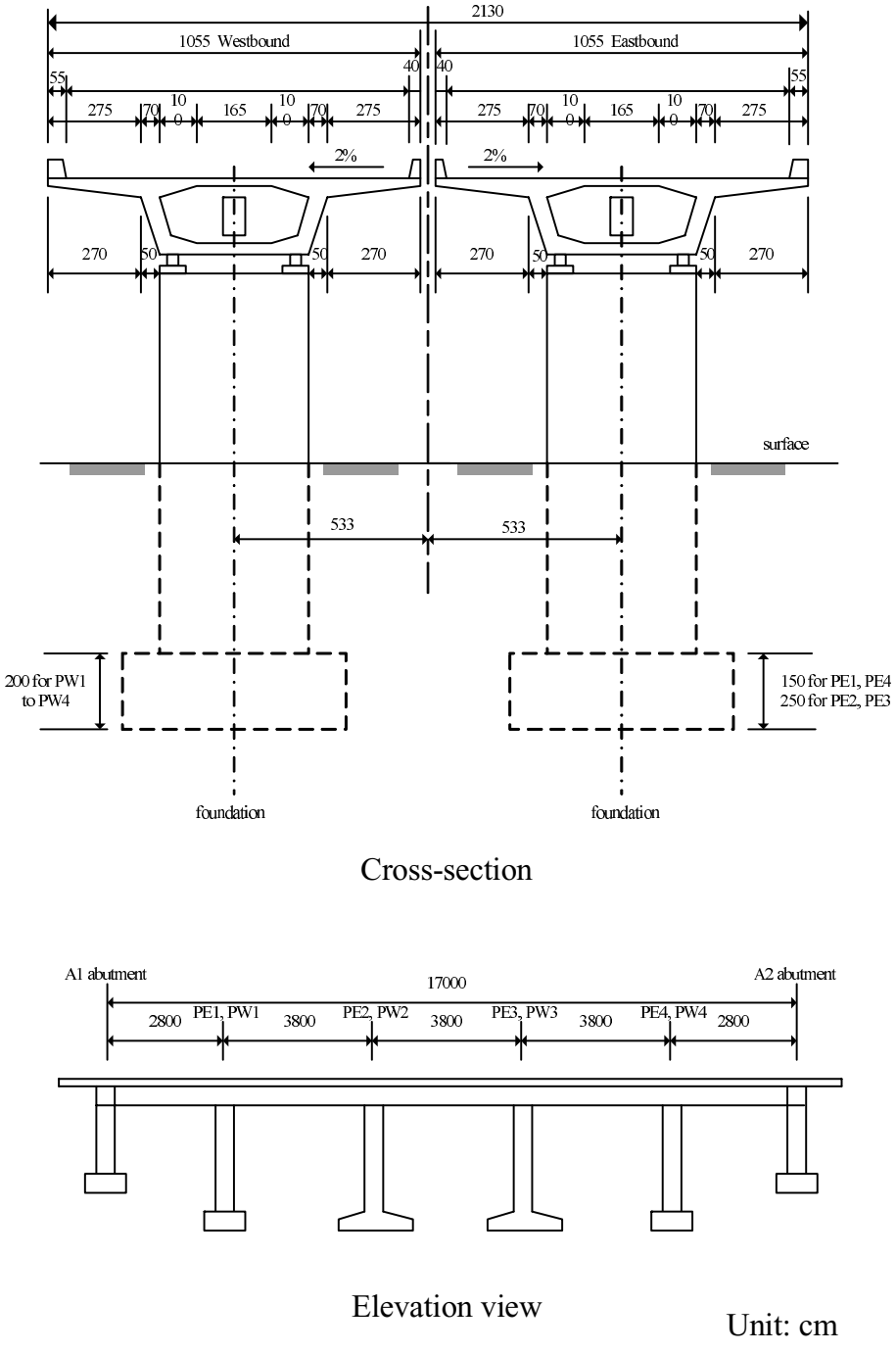

Fig. 1. Cross-section and elevation view of the bridges.

As for the substructure, there are four wall piers (PW1∼PW4) for the west-bounded bridge that have the same size with cross-section dimension of 1.2 m × 4.05 m. Lead rubber bearings (LRB) are installed on the piers to form an isolated bridge. However, conventional rubber bearings are installed on the abutments.

The east-bounded bridge was designed to be conventional. All four piers have the same cross-section dimension of 1.4 m × 4.05 m. The conventional pot bearings on the first and the fourth piers (PE1 and PE4) are fixed. The

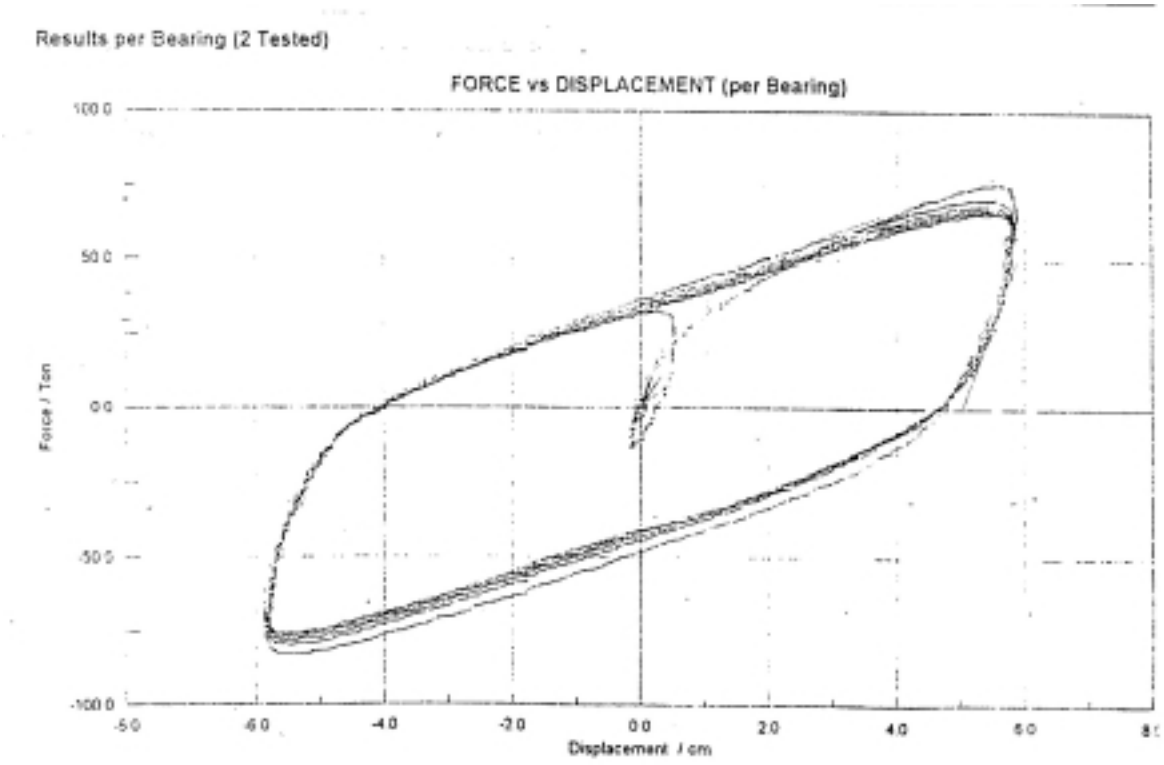

Fig. 2. Hysteretic loop of lead rubber bearing.

bearings on the second and the third piers (PE2 and PE3) are free in longitudinal direction.

The size of the lead rubber bearing adopted on the isolated bridges is as follows: total height is 233 mm, the plane dimension is 875 $\times$ 875 mm, the size of the stiffened steel plate is 855 $\times$ 855 mm, and the diameter of the lead core is 4@105 mm. There are 7 rubber layers, with a thickness of 13 mm each. The full-scale test of the LRB was conducted in Wellington, New Zealand, including the compressive test, the pressure/shearing force load test (axial load is 361 tons, deformation is 59 mm, repeated load frequency is 0.04 Hz). Six samples were tested and the results are shown in Fig. 2.

The construction of the bridges started in 1998. They underwent both the Chi-Chi earthquake (September 21, 1999) and the Chi-I earthquake (October 22, 1999) and were partially damaged during the construction period. Repairs were completed the following year, and the bridges were officially finished and open to traffic in 2001. Several field tests were conducted during this period. These tests showed interesting results and were compared with theoretical simulation.

3. Ambient vibration test

The ambient vibration test included the surroundings test and the bridge test. The surrounding ambient vibration test was firstly carried out before the bridge was constructed, and then was carried on after each ambient vibration test. The goal was to verify the soil-structure interaction, to identify the structural mode and to modify the structural model accordingly.

The ambient vibration tests were conducted in the three stages during bridge construction: (a) the pier was constructed, but the bearing was not installed yet. The sensors were installed on the top of the pier. (b) The bearings were installed, but the bridge deck was not constructed yet. The sensors were installed on the top of the bearing. (c) The bridge structure was completed, but the asphalt was not paved yet. The sensors were installed on the deck.

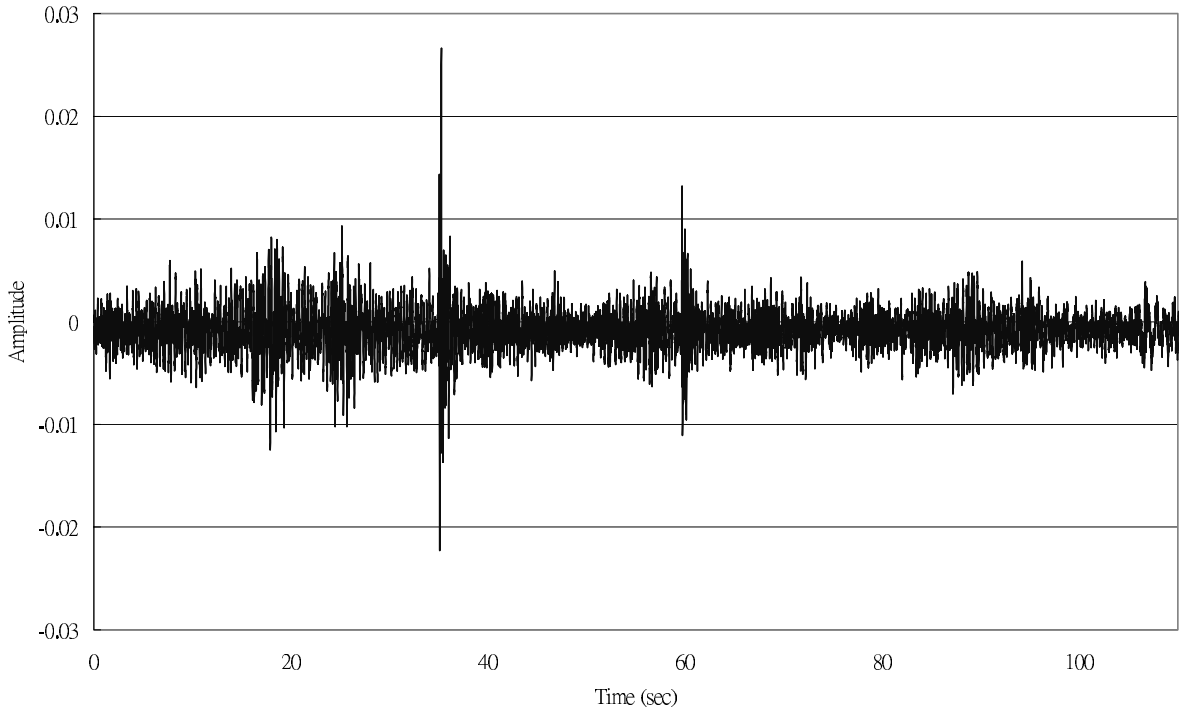

Fig. 3. Signal collected from ambient vibration test.

Velocimeters were well arranged at appropriate positions to collect the signals so that the dynamic properties of the bridge could be obtained.

3.1. Analysis of signals

To identify the frequencies of the structure, the signals collected in the time domain as shown typically in Fig. 3 were transformed to the frequency domain by using Fast Fourier Transform (F.F.T.), and is shown in Fig. 4. There are many peaks appeared in the Fourier spectrum diagram due to the disturbance and noise in the field. The dominant frequencies are difficult to be identified unless the noise can be filtered out properly.

The Power Spectrum method [10] is adopted to filter out the disturbance and noise and to clarify the structural frequencies as follows:

The energy of signal within $t = \pm\infty$ is

$$e_{xx} = \int_{-\infty}^{\infty} x(t)x^*(t)dt \tag{1}$$

Define the correlated energy of two signals x and y as

$$e_{xy}(\tau) = \int_{-\infty}^{\infty} x(t)y^*(t-\tau)dt \tag{2}$$

$$e_{yx}(\tau) = \int_{-\infty}^{\infty} y(t)x^*(t-\tau)dt = e^*_{xy}(-\tau) \tag{3}$$

The energy spectrum is defined as

$$E_{xx}(i\omega) = X(i\omega)X^*(i\omega) \tag{4}$$

After using F.F.T., the orthogonal power energy definition of signals x and y is

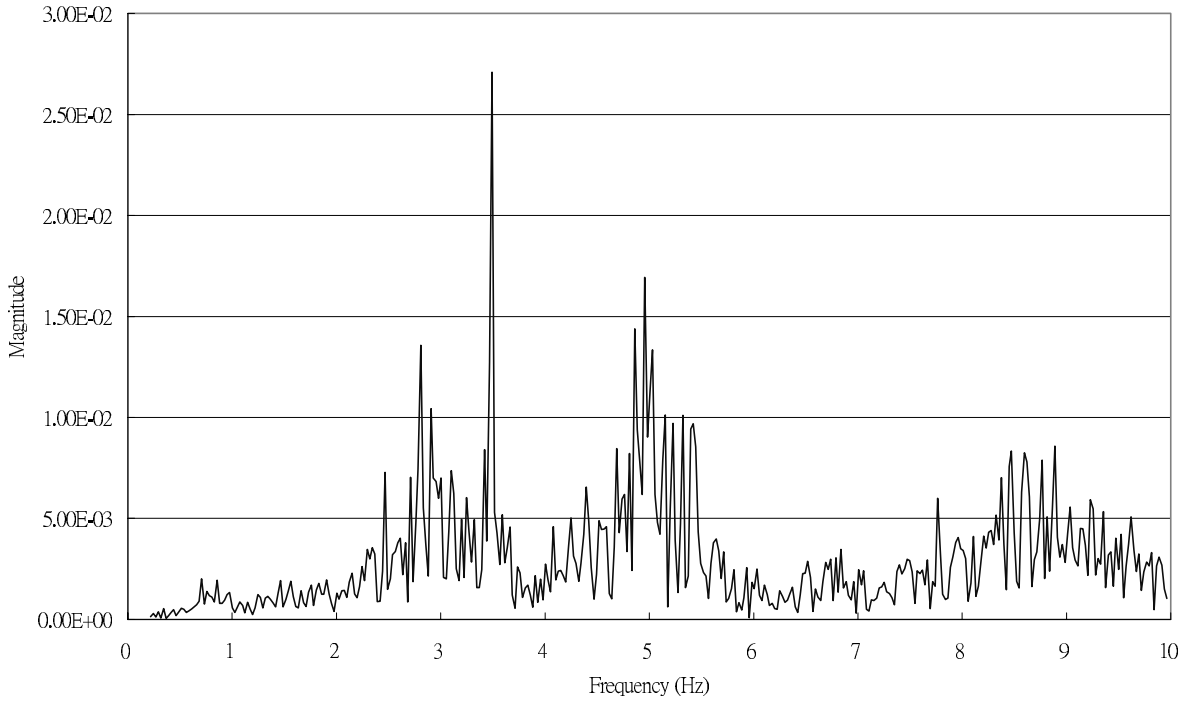

Fig. 4. Fourier spectrum.

$$E_{xy}(i\omega) = X(i\omega)Y^*(i\omega) \tag{5}$$

From the Parseval relations in Fourier transform, the total sum of energy of signal is

$$\int_{-\infty}^{\infty} x(t)y^*(t)dt = \frac{1}{2\pi}\int_{-\infty}^{\infty} X(i\omega)Y^*(i\omega)d\omega \tag{6}$$

It is seen that the signal energy is independent in both time-domain and frequency-domain.

According to the Plancherel theorem, the product of the Fourier transformation of two signals is equal to the Fourier transformation of the convolution integral of these signals in time-domain:

$$\begin{aligned} E_{xy}(i\omega) &= X(i\omega)Y^*(i\omega) \\ &= F\{x\}\cdot F\{y^*\} \\ &= F\left\{\int_{-\infty}^{\infty} x(t)y^*(t-\tau)d\tau\right\} \\ &= F\left\{e_{xy}(\tau)\right\} \end{aligned} \tag{7}$$

If signals x and y are not correlated, it implies that the correlated energy$e_{xy}(\tau) = 0$ at $t = \tau$.

Equation (5) can then be written as:

$$\begin{aligned} E_{xy}(i\omega) &= X(i\omega)Y^*(i\omega) \\ &= \text{real}[X(i\omega)]\cdot\text{real}[Y(i\omega)] + \text{image}[X(i\omega)]\cdot\text{image}[Y(i\omega)] \\ &\quad -\text{real}[X(i\omega)]\cdot\text{image}[Y(i\omega)]i + \text{real}[Y(i\omega)]\cdot\text{image}[X(i\omega)]i \end{aligned} \tag{8}$$

$$\begin{aligned} E_{yx}(i\omega) &= Y(i\omega)X^*(i\omega) \\ &= \text{real}[X(i\omega)]\cdot\text{real}[Y(i\omega)] + \text{image}[X(i\omega)]\cdot\text{image}[Y(i\omega)] \\ &\quad +\text{real}[X(i\omega)]\cdot\text{image}[Y(i\omega)]i - \text{real}[Y(i\omega)]\cdot\text{image}[X(i\omega)]i \end{aligned} \tag{9}$$

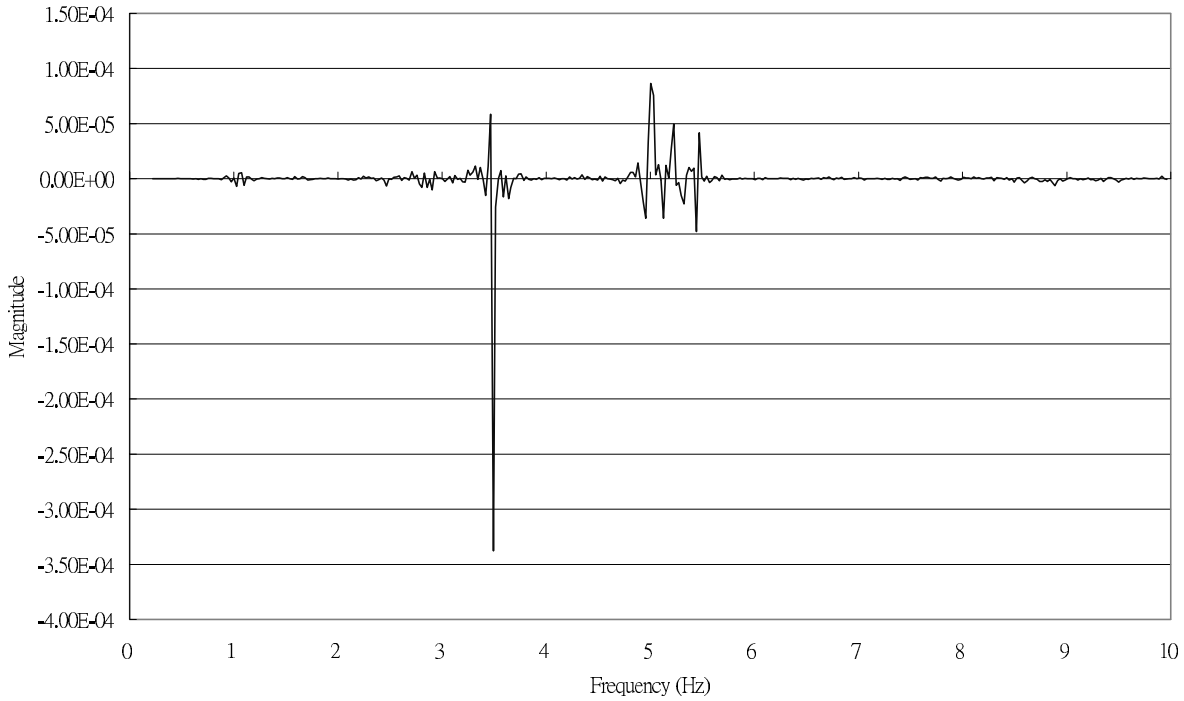

Fig. 5. Phase-amplitude relationship.

Fig. 6. Damage of pot bearing of the east-bounded bridge.

Since signals x and y are independent to their order, $E_{xy} = E_{yx}$:

$$E_{xy}(i\omega) = E_{yx}(i\omega) = \text{real}\,[X(i\omega)] \cdot \text{real}\,[Y(i\omega)] + \text{image}\,[X(i\omega)] \cdot \text{image}\,[Y(i\omega)] \tag{10}$$

Pairs of signals were collected in the test. Measurements were obtained at nearly the same position twice in pair. Since the ambient excitation and the noise for each pair of the measurements is not correlated, according to the characteristics that energy $e_{xy}(\tau) = 0$, and applying Eq. (10), the noise in the Fourier spectrum can be eliminated and the structural frequencies were distinct, as shown typically in Fig. 5.

Table 1
Frequencies obtained from the ambient vibration tests

west-bounded bridge	Longitudinal (Hz)	Transverse (Hz)	Vertical (Hz)
1999/6/26	2.61	2.91	3.49
1999/10/19	2.25	2.76	3.52
1999/11/2	2.05	2.59	3.54
2000/5/8	2.49	2.69	3.54
east-bounded bridge	Longitudinal (Hz)	Transverse (Hz)	Vertical(Hz)
1999/10/19	3.69	3.15	3.52
1999/11/2	3.64	3.20	3.49
2000/5/8	3.96	3.30	3.52

Fig. 7. Damage of RB on the abutment of the west-bounded bridge.

3.2. Results

The ambient vibration tests were conducted during the period from June 16, 1998 to May 8, 2000.

The ambient vibration test on the deck of the west-bounded bridge had been performed, but that of the east-bounded had not been carried out in time, and the bridges underwent the Chi-Chi earthquake on September 21, 1999. And then, after measuring the ambient vibration of the east-bounded and west-bounded bridges on October 19, the bridge underwent another strong earthquake, the Chia-I earthquake, on October 21, 1999.

Several pot bearings on the pier and abutment of the east-bounded, and the rubber bearings on the abutment of the west-bounded, were distorted significantly after the earthquakes as shown in Figs 6 and 7. However, none of the lead rubber bearing was damaged.

The scheduled dynamic test was postponed until May 8, 2000, after the bridges were retrofitted and the damaged bearings were replaced.

Results of each ambient vibration test are summarized in Table 1 and are shown in Figs 8 to 16. Figure 17 shows the conduction of an ambient vibration test on the bridge deck after the main bridge structure was constructed.

As seen in Table 1, the longitudinal and transverse frequencies of the west-bounded bridge decreased significantly after the Chi-Chi earthquake. However, the frequency was restored to as before the earthquake after the rubber bearings were replaced. The variation of frequencies is shown in Fig. 18.

We were not able to measure the response of the east-bounded bridge structure in time before the Chi-Chi earthquake. However, by comparing the frequency of the bridge before and after the Chia-I earthquakes, it was observed that the frequency decreased slightly after the earthquake, as shown in Fig. 19. It is because the pot bearings on the top of the abutment and PE1 were damaged due to the strong earthquakes. After the pot bearings were replaced, the longitudinal and transverse frequencies rose.

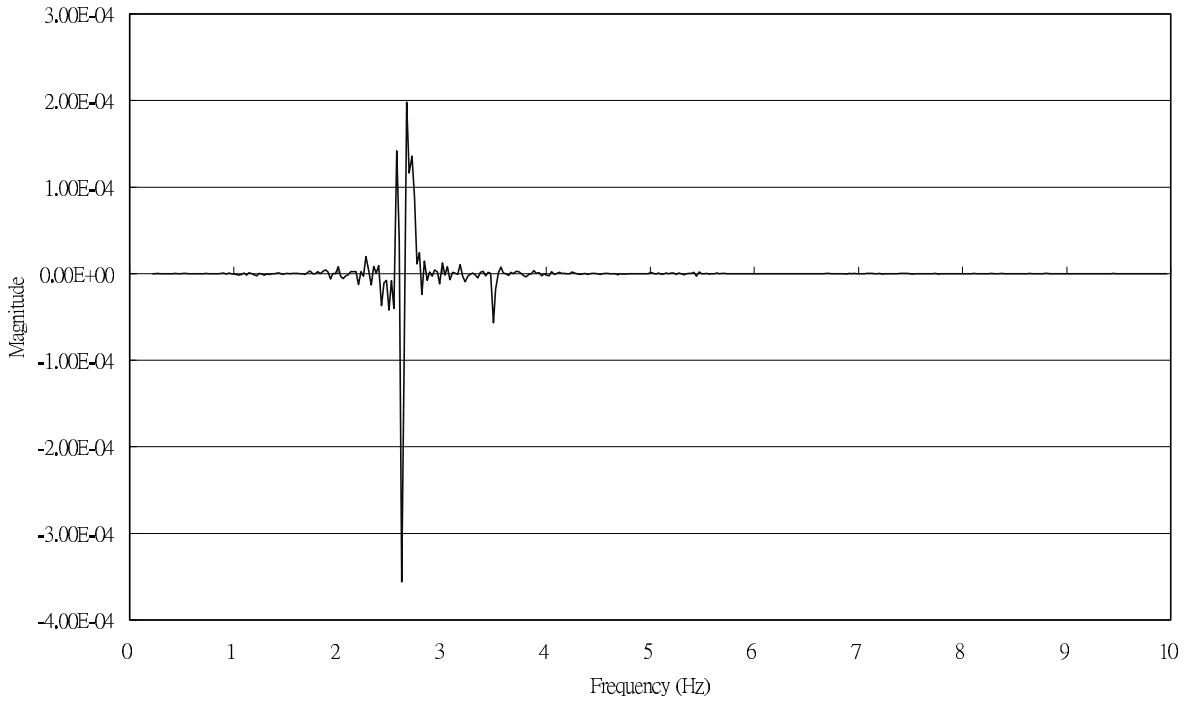

Fig. 8. Phase-amplitude relationship of ambient vibration in longitudinal direction of west-bounded bridge on 1999/6/26.

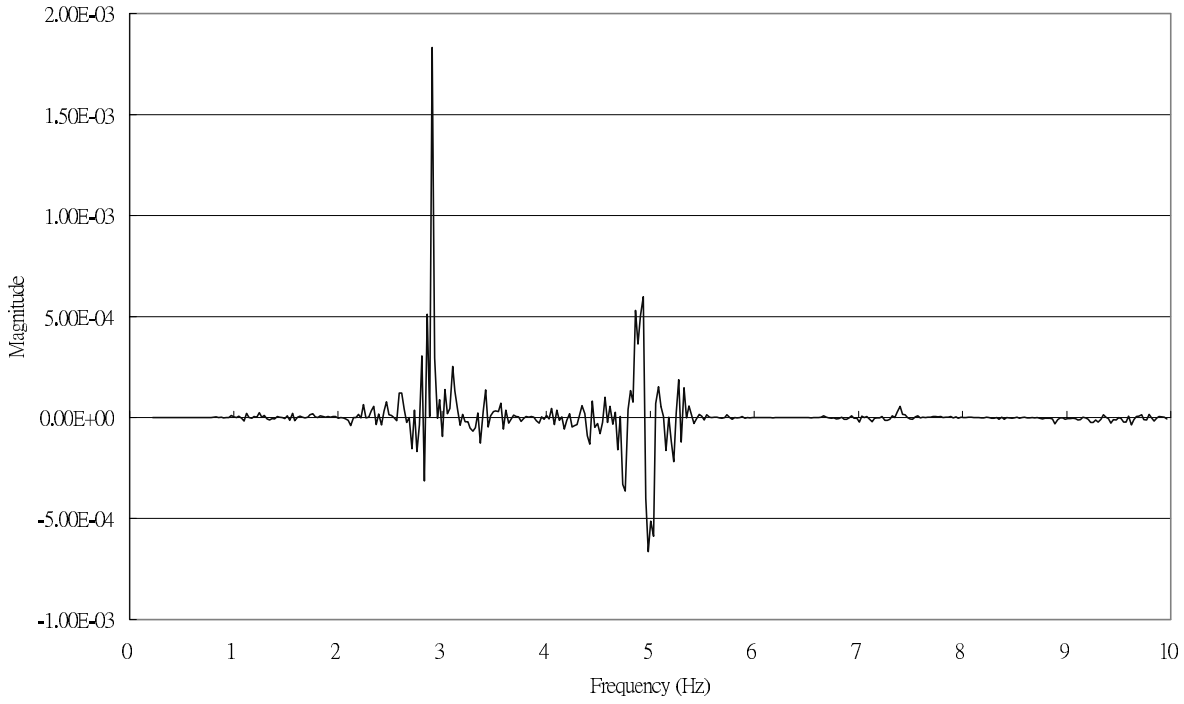

Fig. 9. Phase-amplitude relationship of ambient vibration in transverse direction of west-bounded bridge on 1999/6/26.

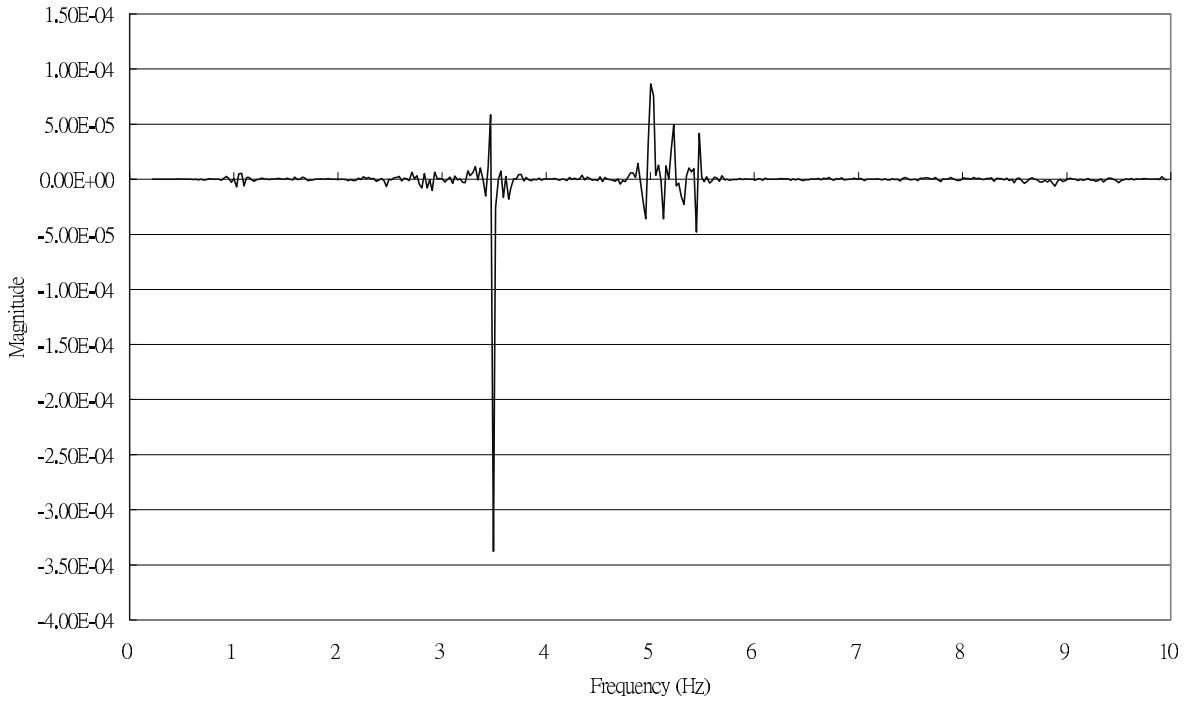

Fig. 10. Phase-amplitude relationship of ambient vibration in vertical direction of west-bounded bridge on 1999/6/26.

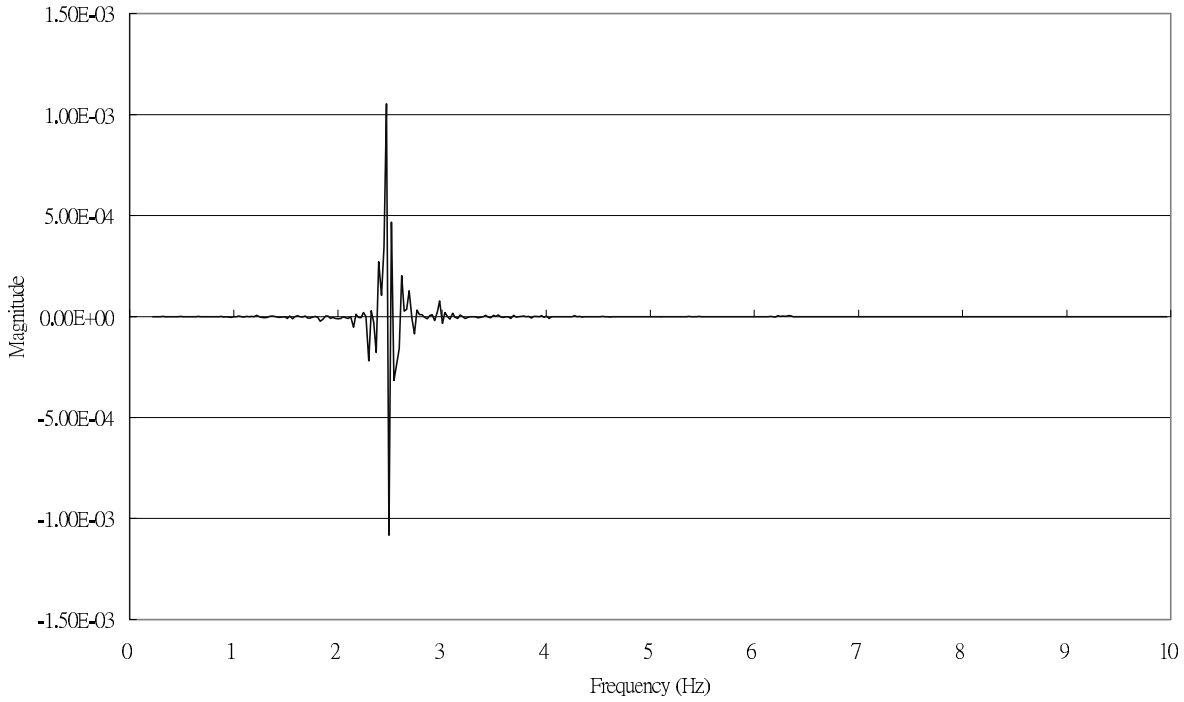

Fig. 11. Phase-amplitude relationship of ambient vibration in longitudinal direction of west-bounded bridge on 2000/5/8.

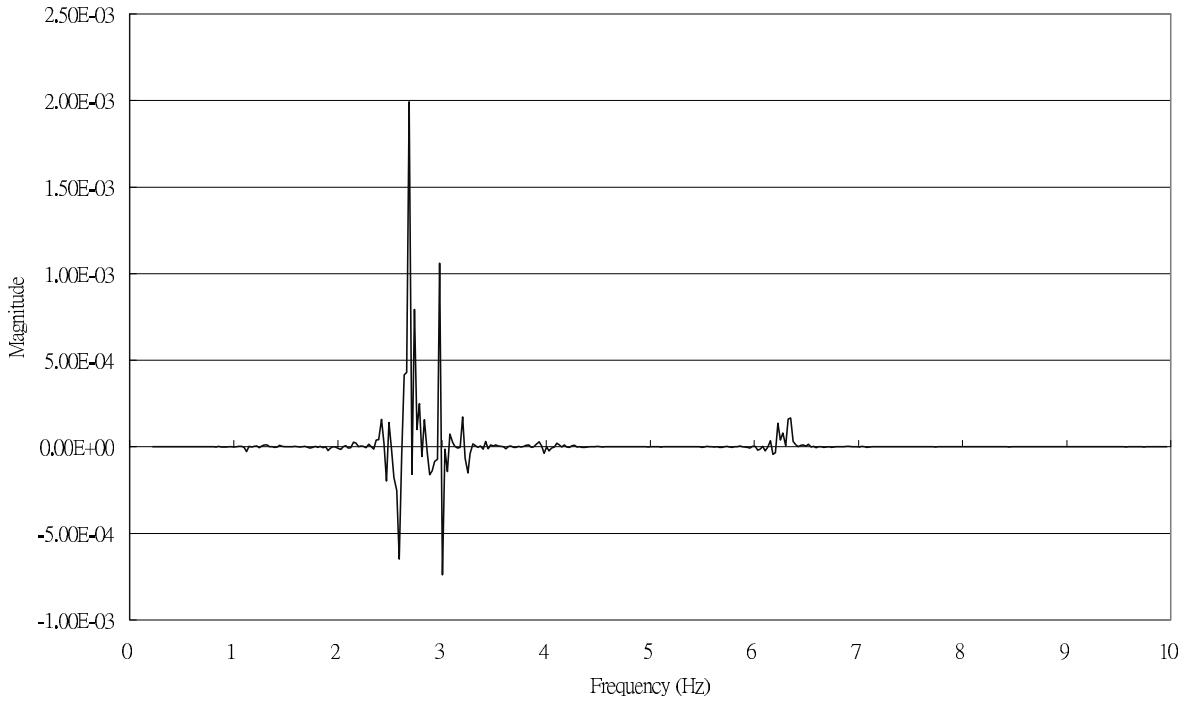

Fig. 12. Phase-amplitude relationship of ambient vibration in transverse direction of west-bounded bridge on 2000/5/8.

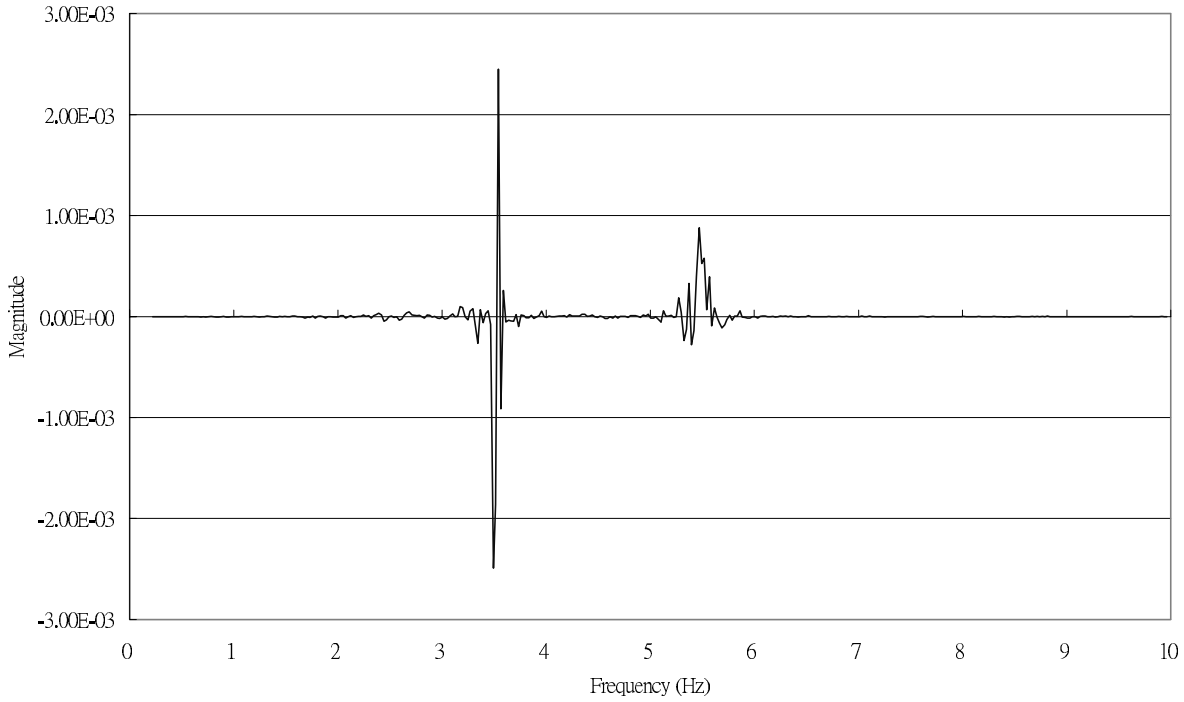

Fig. 13. Phase-amplitude relationship of ambient vibration in vertical direction of west-bounded bridge on 2000/5/8.

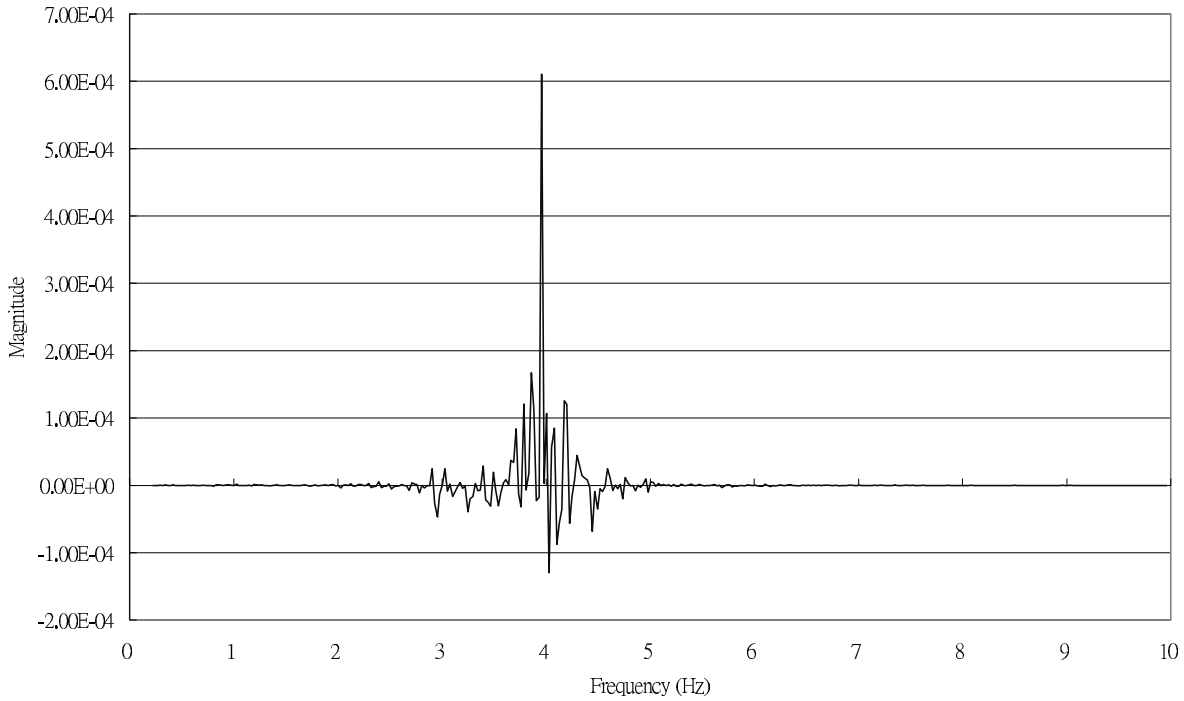

Fig. 14. Phase-amplitude relationship of ambient vibration in longitudinal direction of east-bounded bridge on 2000/5/8.

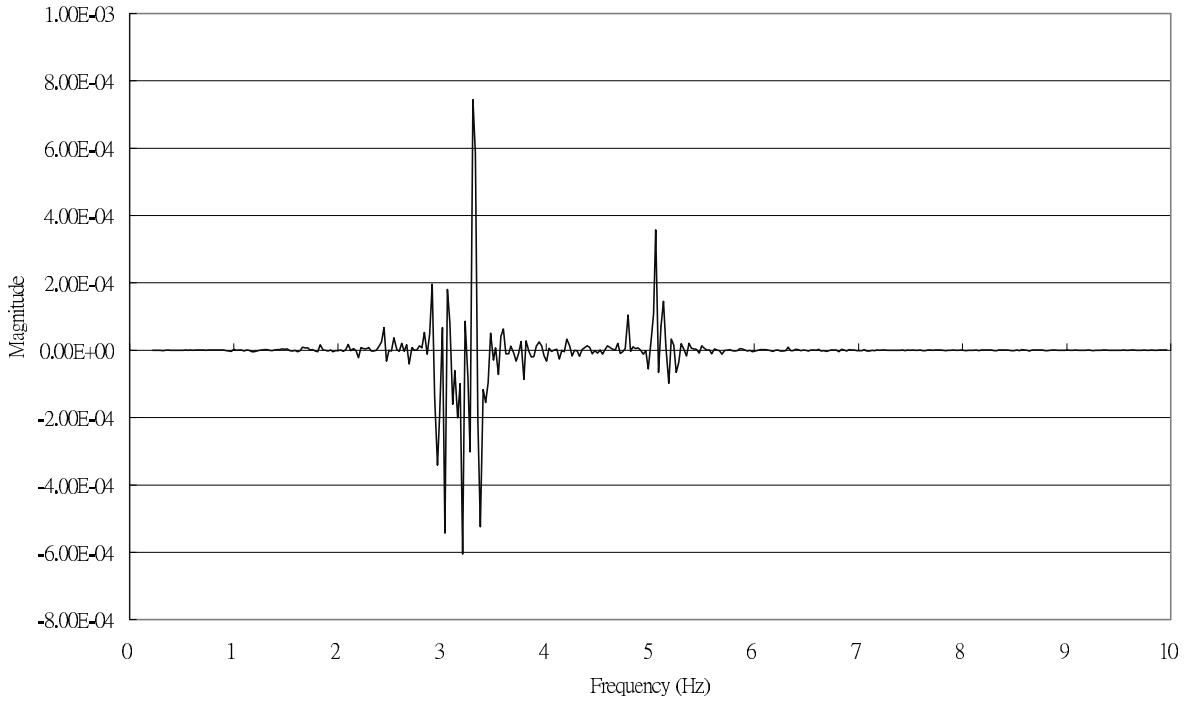

Fig. 15. Phase-amplitude relationship of ambient vibration in transverse direction of east-bounded bridge on 2000/5/8.

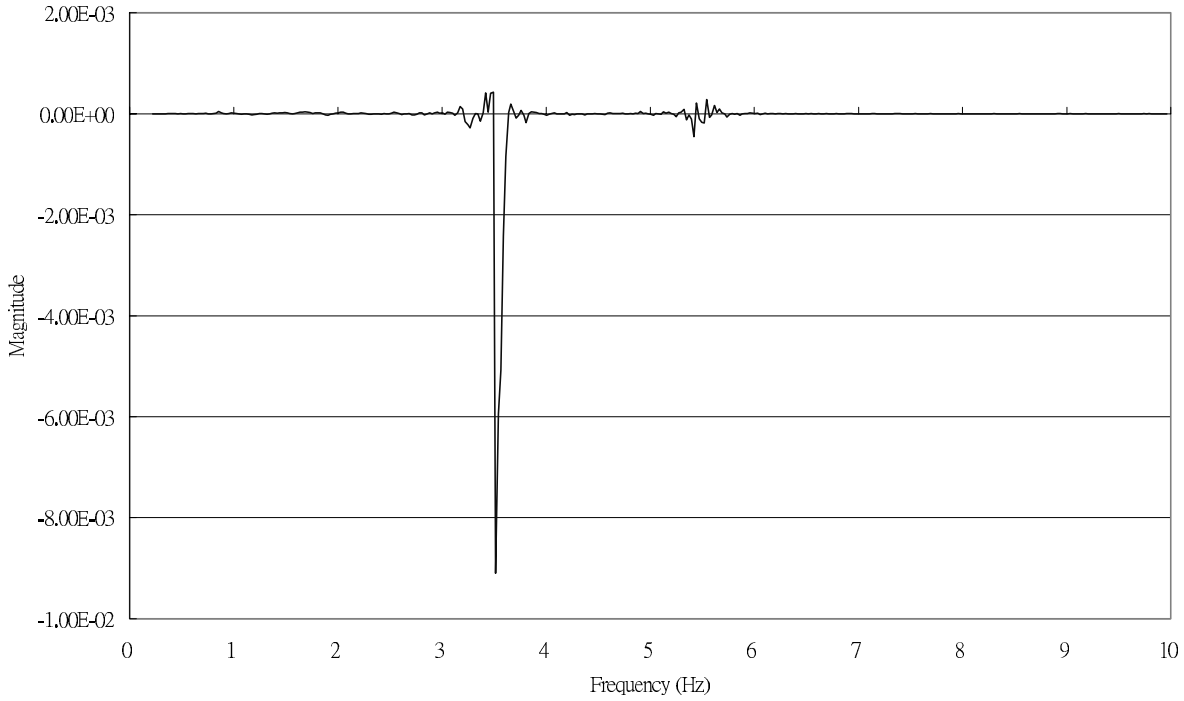

Fig. 16. Phase-amplitude relationship of ambient vibration in vertical direction of east-bounded bridge on 2000/5/8.

Fig. 17. Ambient vibration test of bridges.

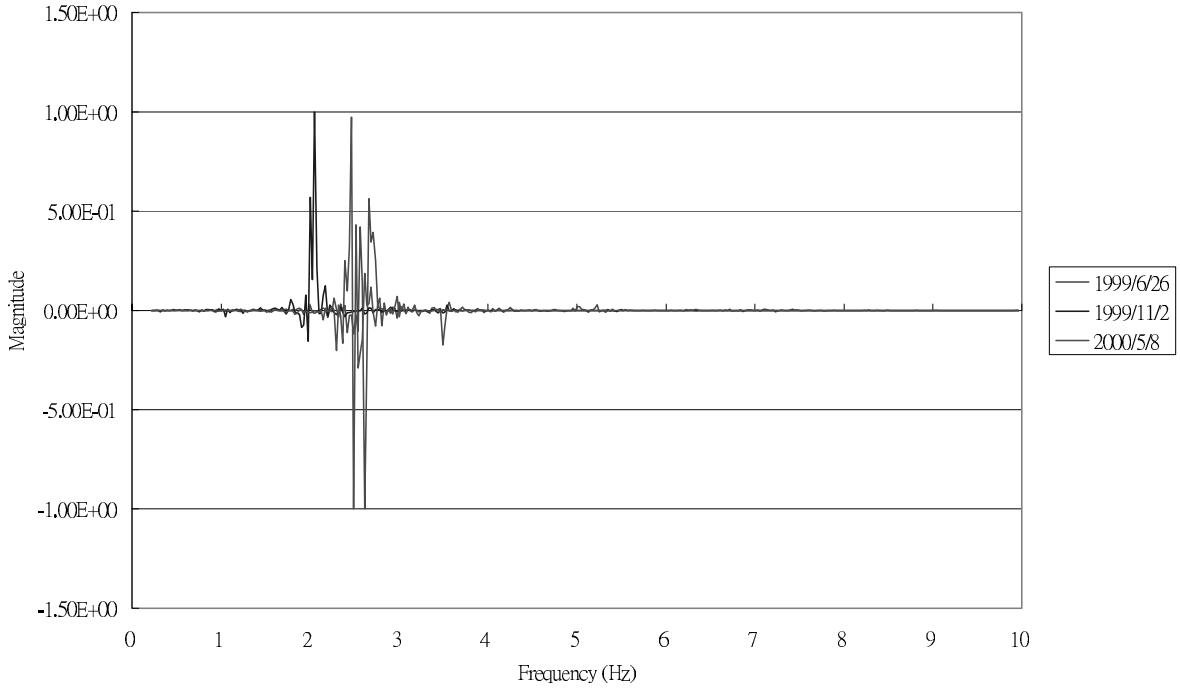

Fig. 18. Variation of frequencies before damage, after damage and after retrofitting of the west-bounded bridge.

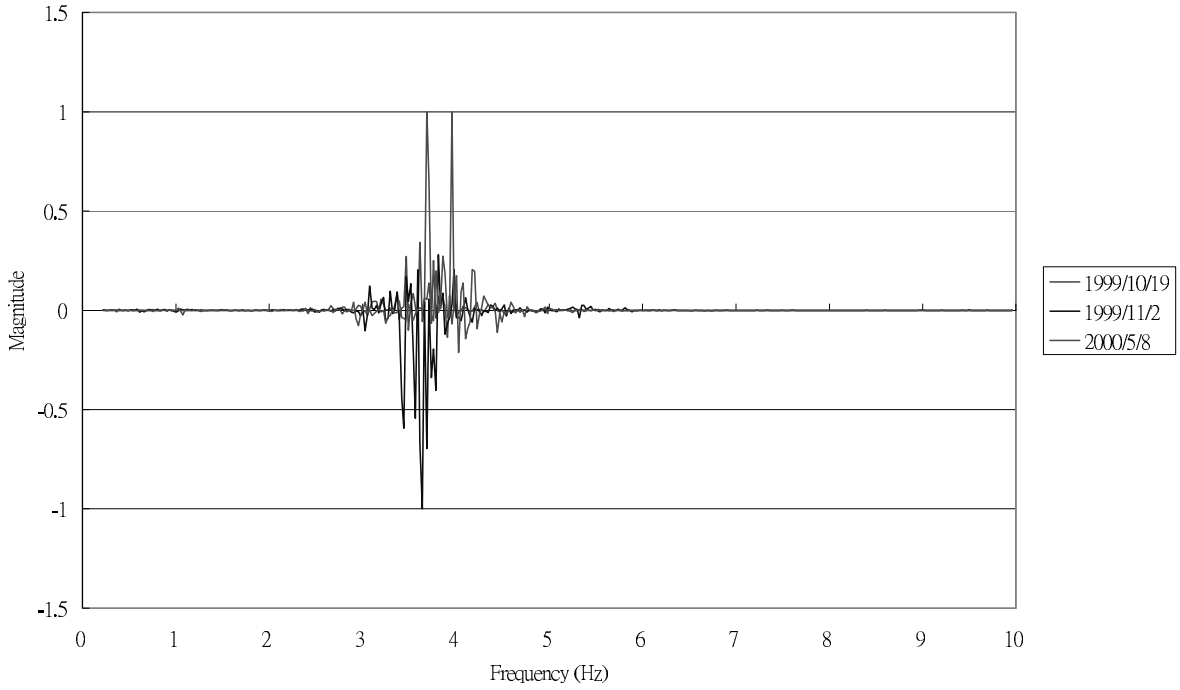

Fig. 19. Variation of frequencies before and after damage and after retrofitting of the east-bounded bridge.

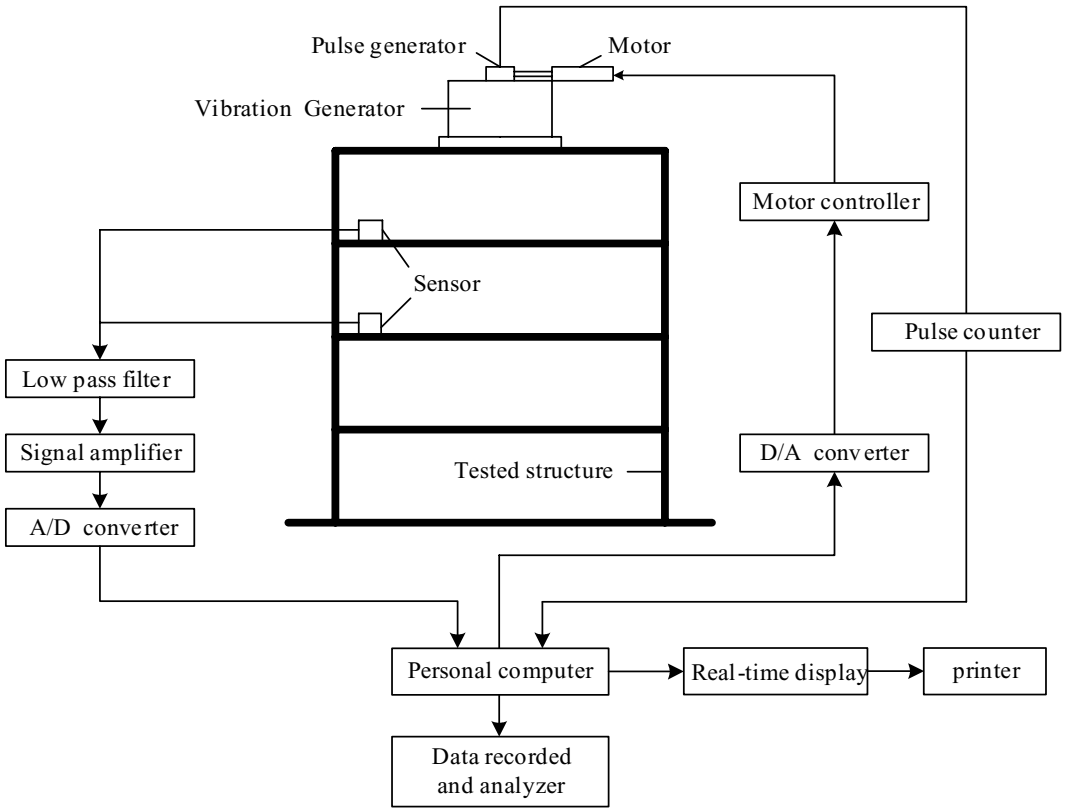

Fig. 20. Block diagram of the force vibration test system.

It is noted that the damage of the bearings could cause the change of frequency and can be shown in the ambient vibration test.

4. Force vibration test

Shakers are placed on the decks of east-bounded and the west-bounded bridges, respectively. The shakers can produce sinusoidal force with different frequencies and excite the bridge to vibrate. The frequency, damping ratio, and modal shape of the bridge can be measured accordingly.

In order to make the shaker stable on the bridge deck during vibration, and transmit the force induced by the shaker to the bridge deck smoothly, concrete blocks were used to grout on the third span of the deck of the west-bounded and east-bounded bridges, respectively, during the construction of bridge decks.

Shakers, part of the sensors, as well as the instruments and control system were all on loan from the National Center for Research on Earthquake Engineering (NCREE). The NCREE also supported technician manpower and assisted with the conduction of the test.

4.1. Testing system

The block diagram in Fig. 20 shows the testing system. The system can be divided into three parts. The blocks denoted by “Vibration Generator” down to “Personal Computer” on the right-hand side of the diagram represent the “harmonic vibration force generating equipment”. The blocks denoted by “sensor”, “filter” and “amplifier” on the left-hand side of the diagram represent the equipment for measuring the response of the structure. Finally, the blocks from “A/D converter” to “Data storage and analysis” are the data recording and analysis equipment. It should be

Table 2
The specification of shakers

Type	MK-4600		MK-460
Force Direction	Longitudinal	Transverse	Vertical
Rotational Speeds (Hz)	$0.5 \sim 9.5$	$0.5 \sim 9.1$	$3.0 \sim 10.0$
Maximum Force (lb)	10000	10000	10000
Eccentricity (%)	100 \ 40 \ 20		100 \ 80 \ 60

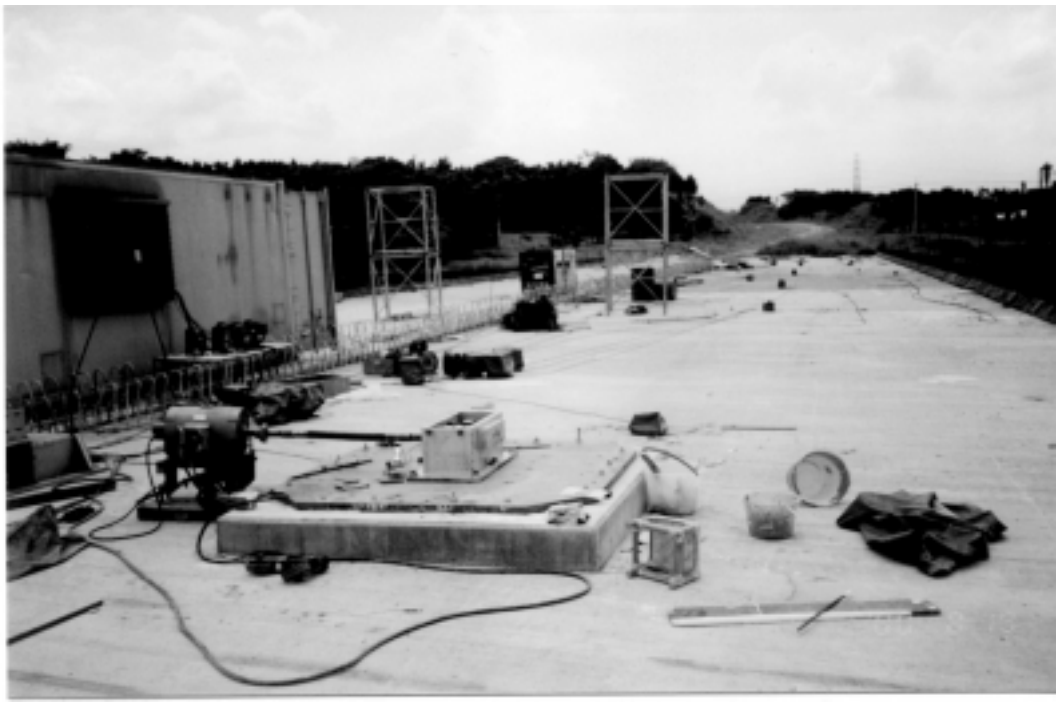

Fig. 21. Force vibration test in the vertical direction by MK-460.

noted that the "Pulse generator" is used to periodically send out a pulse signal when the harmonic force generated by the vibration functions reaches its maximum value. The purposes of the pulse generator are: (1) to obtain the phase angle of the structure response, and (2) to serve as the feedback signal for automatically controlling the rotating speed of the vibration generator.

The NCREE has two types of vibration generator of eccentric rotating mass, which are made by the ANCO Company. They are models MK-4600 and MK-460, respectively. The former can induce horizontal sinusoidal force while the latter can induce vertical sinusoidal force (see Table 2 for the specifications). For both types, a uni-direction harmonic force is produced by symmetrically rotating two eccentric masses inside the vibration generators.

The force generated by the shaker is constant, which is related to the eccentric moment and rotation speed as follows:

$$\text{shaker } force = 0.102 \times eccentric\, moment \times rotation\ speed^2 \tag{11}$$

Shown in Fig. 21 is the appearance of the vibration generator model MK-4600, and Fig. 22 is model MK-460.

4.2. Steps of the test

Sixteen sensors were installed on the bridge deck and on the top of piers. Accelerometers, used as sensors, can measure the response of the bridge vertically or horizontally depending on its measuring direction.

Fig. 22. Force vibration test in the horizontal direction by MK-4600.

The shakers are fixed firmly in positions on the concrete block by bolts. We operated model MK-460 shaker to exert vertical sinusoidal force on the west-bounded bridge. When the vibration responses reached a steady state, we started to collect the signal through the computer control system for five minutes.

Then we adjusted the eccentricity of the mass in the shaker so as to change the rotational speed, which is relevant to the frequency, according to Eq. (11). Then we repeated the procedure until the frequency of the force cannot be adjusted further more.

Then we operated model MK-4600 shaker similarly, except that it may exert forces in the longitudinal and transverse directions to the bridge respectively.

After the tests on the west-bounded bridge are completed, we moved all of the instruments to the east-bounded bridge and repeated the same procedure.

The frequency range of the force induced by the shaker is 0.5 to 9.4 Hz in longitudinal direction, 0.5 to 9.5 Hz in transverse direction, and 2.5 to 9.4 Hz in vertical direction for the west-bounded bridge. For the east-bounded, they are 0.5 to 8.7 Hz, 0.5 to 8.2 Hz, and 2.7 to 9.5 Hz, respectively. The reason why the frequency range in vertical direction has to start from 2.5 Hz is that the vertical force is generated by a smaller shaker and it seems that the shaker cannot operate normally at a lower frequency.

4.3. Results

Time history responses were measured by accelerometers and were transformed into frequency domain by FFT. Frequency spectra under excitation forces with various oscillation frequencies were plotted on the same graph, as shown in Figs 23 to 28. The oscillation frequency of the bridge was identified. Adopting the half-power bandwidth method, the damping ratio was derived and is shown in Table 3.

Table 3 shows that the frequencies detected in the forced vibration test are lower than those from the ambient vibration test. This is due to the fact that the ambient excitation is less than the excitation from shakers.

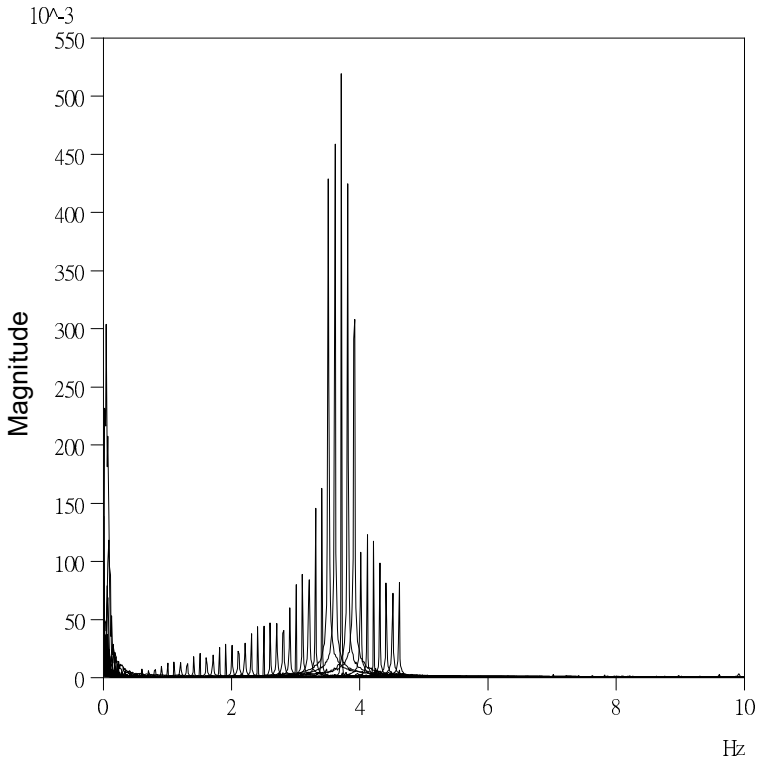

Fig. 23. Frequency responses of force vibration test in longitudinal direction of the east-bounded bridge.

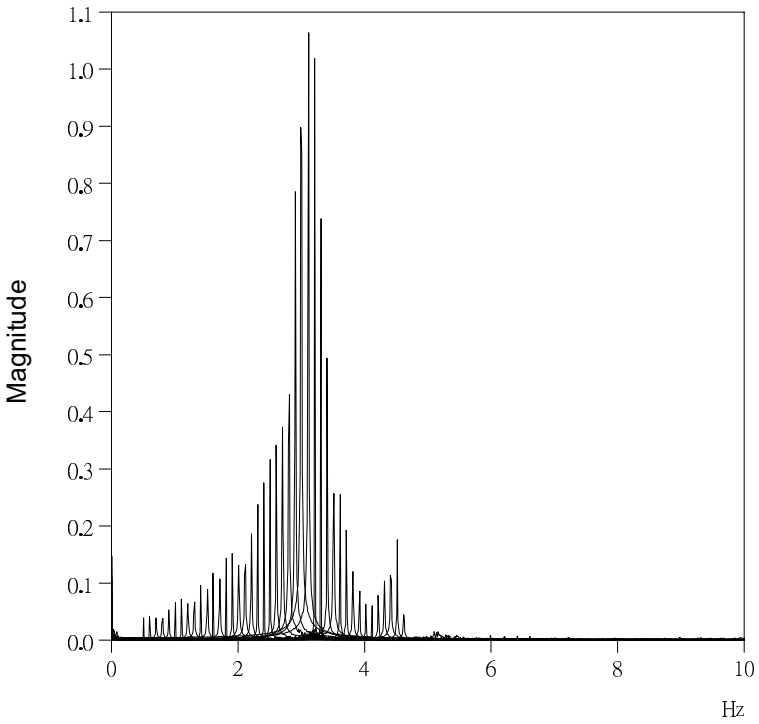

Fig. 24. Frequency responses of force vibration test in transverse direction of the east-bounded bridge.

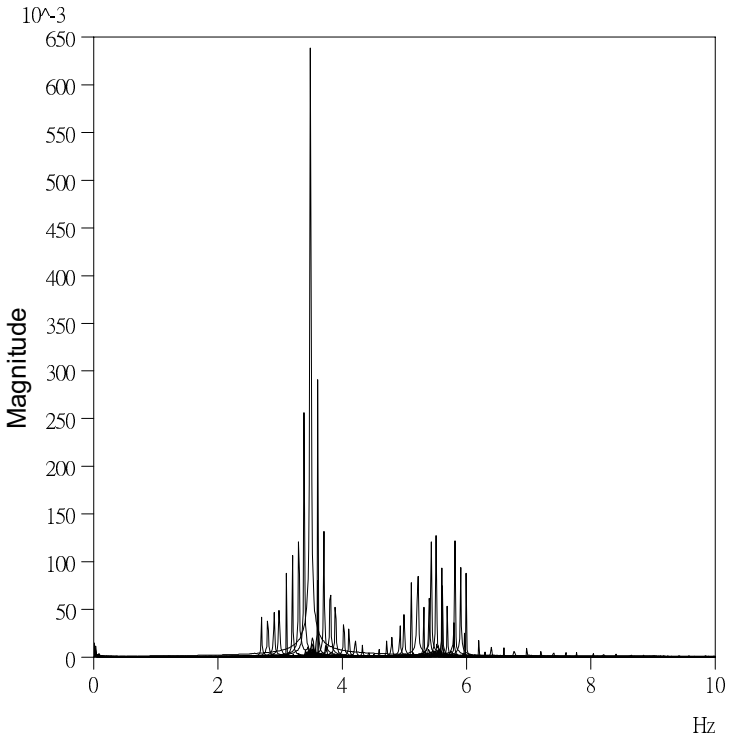

Fig. 25. Frequency responses of force vibration test in vertical direction of the east-bounded bridge.

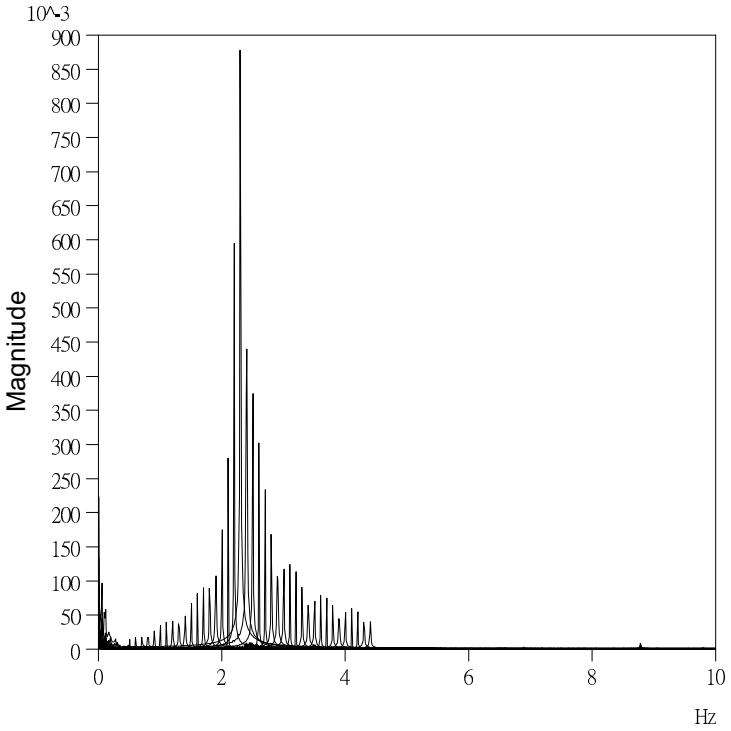

Fig. 26. Frequency responses of force vibration test in longitudinal direction of the west-bounded bridge.

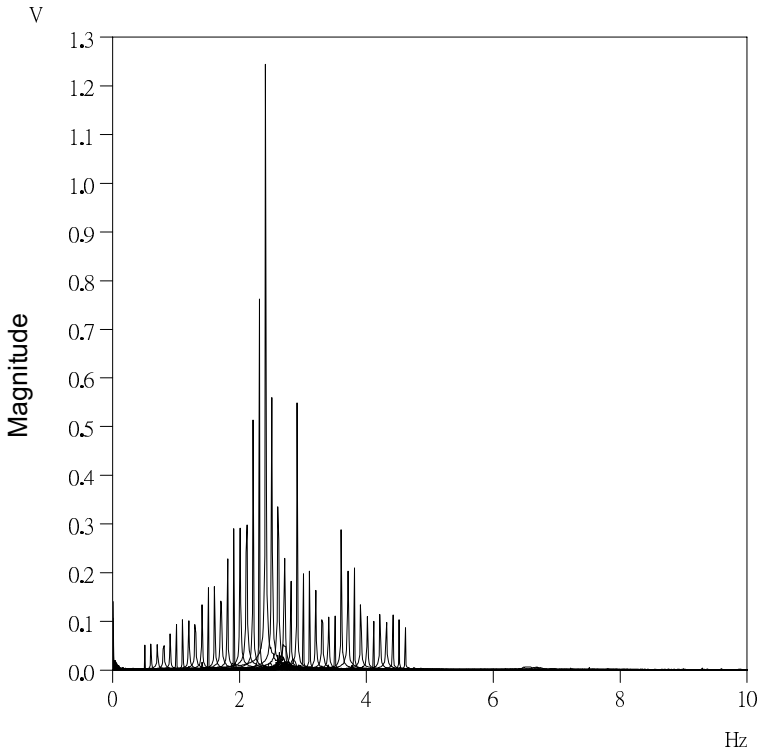

Fig. 27. Frequency responses of force vibration test in transverse direction of the west-bounded bridge.

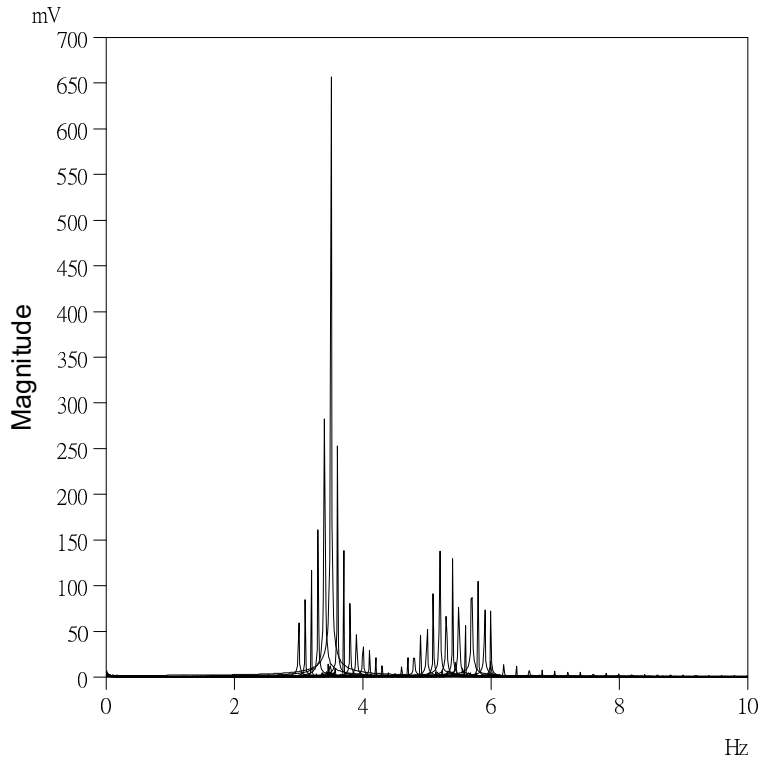

Fig. 28. Frequency responses of force vibration test in vertical direction of the west-bounded bridge.

Table 3
Resonance frequency and damping ratios of bridges identified from force vibration test

	Force direction	Frequency (Hz)	Damping ratio
west-bounded bridge	Vertical	3.5	1.4%
	Longitudinal	2.3	2.95%
	Transverse	2.5	3.2%
East-bounded bridge	Vertical	3.5	1.48%
	Longitudinal	3.7	5.3%
	Transverse	3.2	6.7%

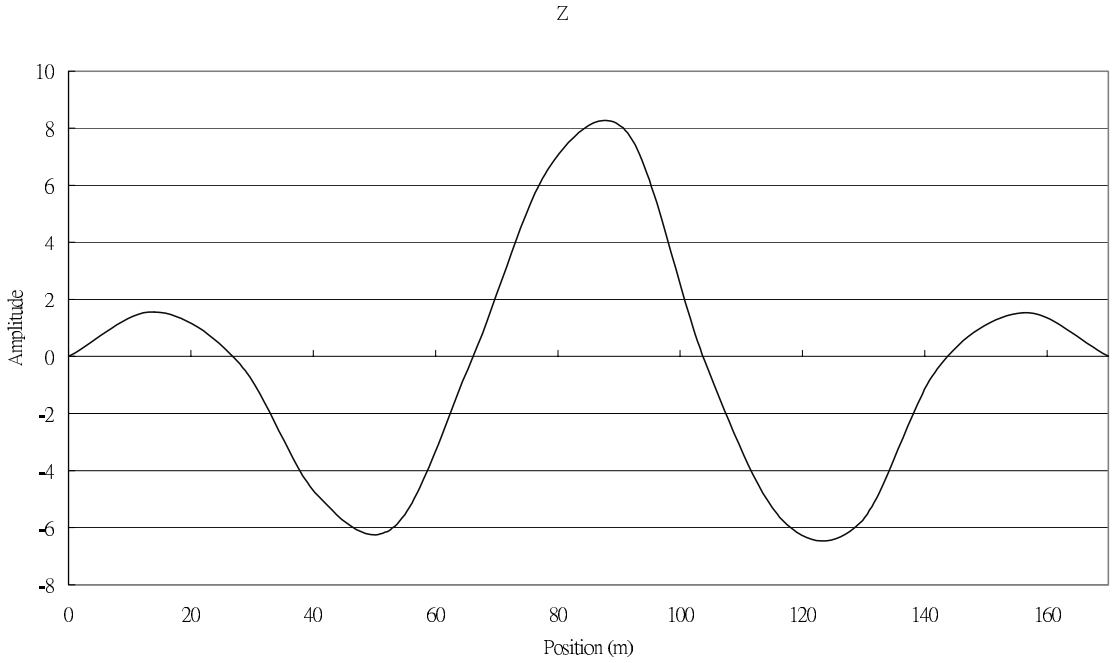

Fig. 29. Mode shape of east-bounded bridge.

The damping ratios of the east-bounded bridge are less than those of the west-bounded. This is due to the hysteretic characteristics of lead rubber bearings. A higher equivalent damping ratio is reflected accordingly in the west-bounded bridge. But in vertical direction, the vertical stiffness of LRB is quite high and so is the traditional pot bearing. Therefore the damping ratios of both bridges are almost the same.

Dominant modal shapes of the east-bounded and west-bounded bridges are shown in Figs 29 and 30, respectively.

5. Free vibration test of the bridge

A push-and-fast-release system was designed to push the decks of both bridges, induce an initial displacement, and release fast. The bridges will therefore vibrate freely.

Because the east-bounded and west-bounded bridges are parallel, the free vibration test can be carried out by pushing both decks of the bridges simultaneously and then releasing immediately. Then both bridges will vibrate freely after their initial displacement.

System sets of well-designed push-and-fast-release are placed between the third piers of the east and the west-bounded bridges (Fig. 31). The hydraulic jack in the system pushes the decks slowly. When the force exerted by the jack approaches our objective magnitude, the jack is released instantly. The free vibration responses of the bridges are measured. This test can detect the main frequencies, the damping ratio, and the modal shapes, etc. of the bridges.

The free vibration test was conducted during the period from August 21, 2000 to September 22, 2000.

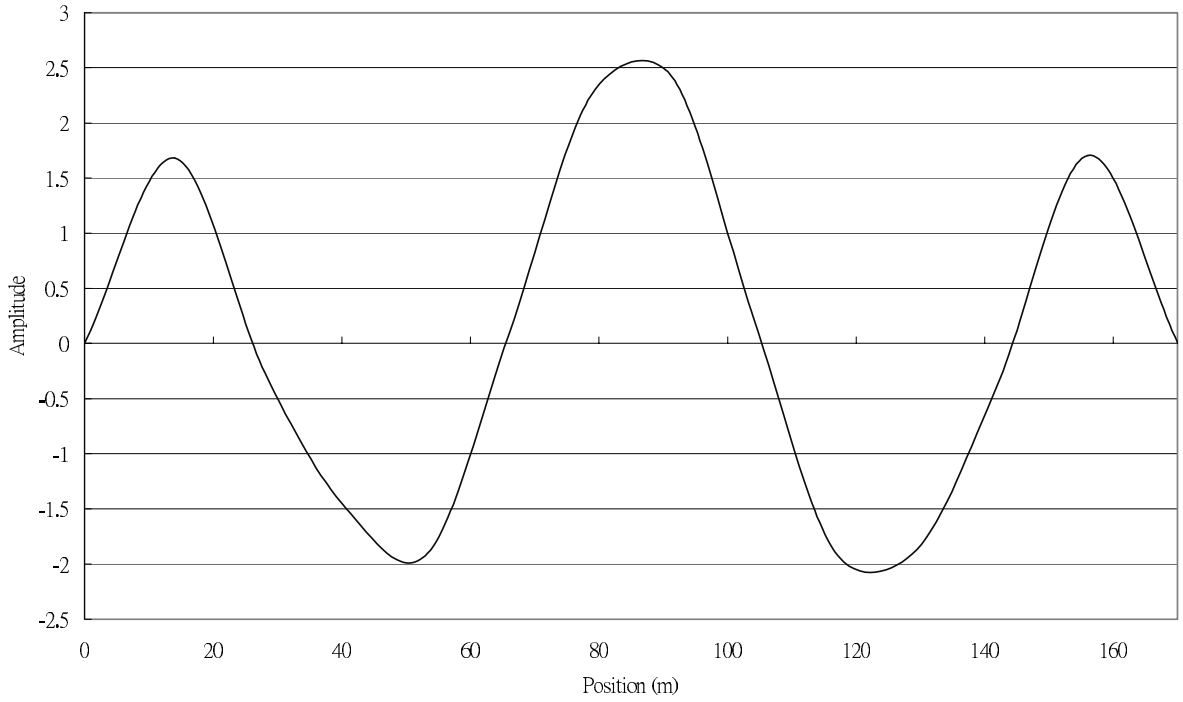

Fig. 30. Mode shape of west-bounded bridge.

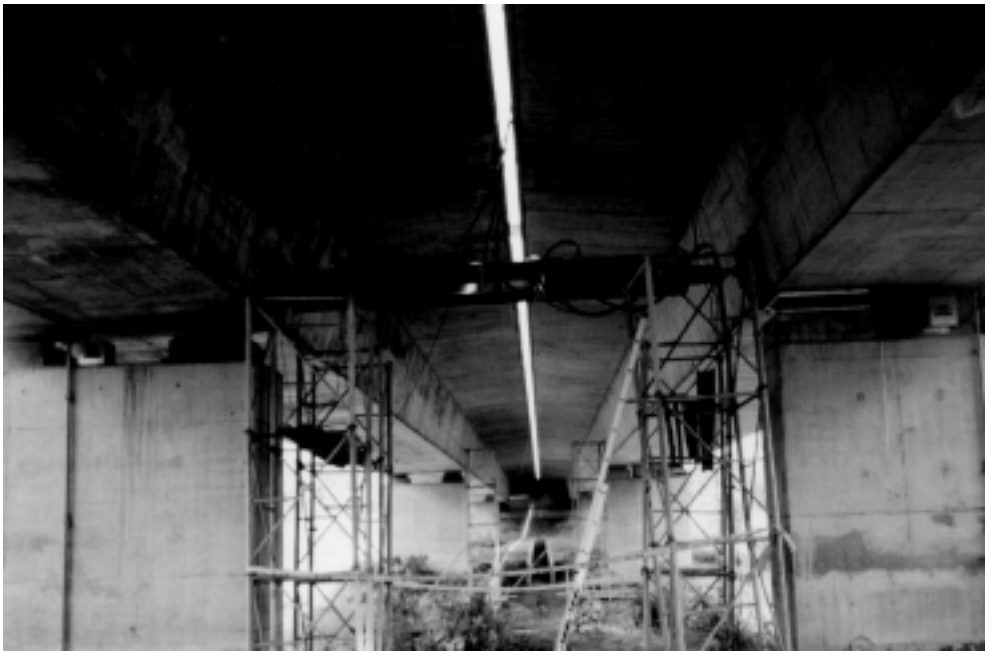

Fig. 31. Push-and-fast-release system.

5.1. Preparation work

In order to prevent the bridges from damages or personnel casualties during the test processes, preparatory work must be planned in detail. The following are four major considerations:

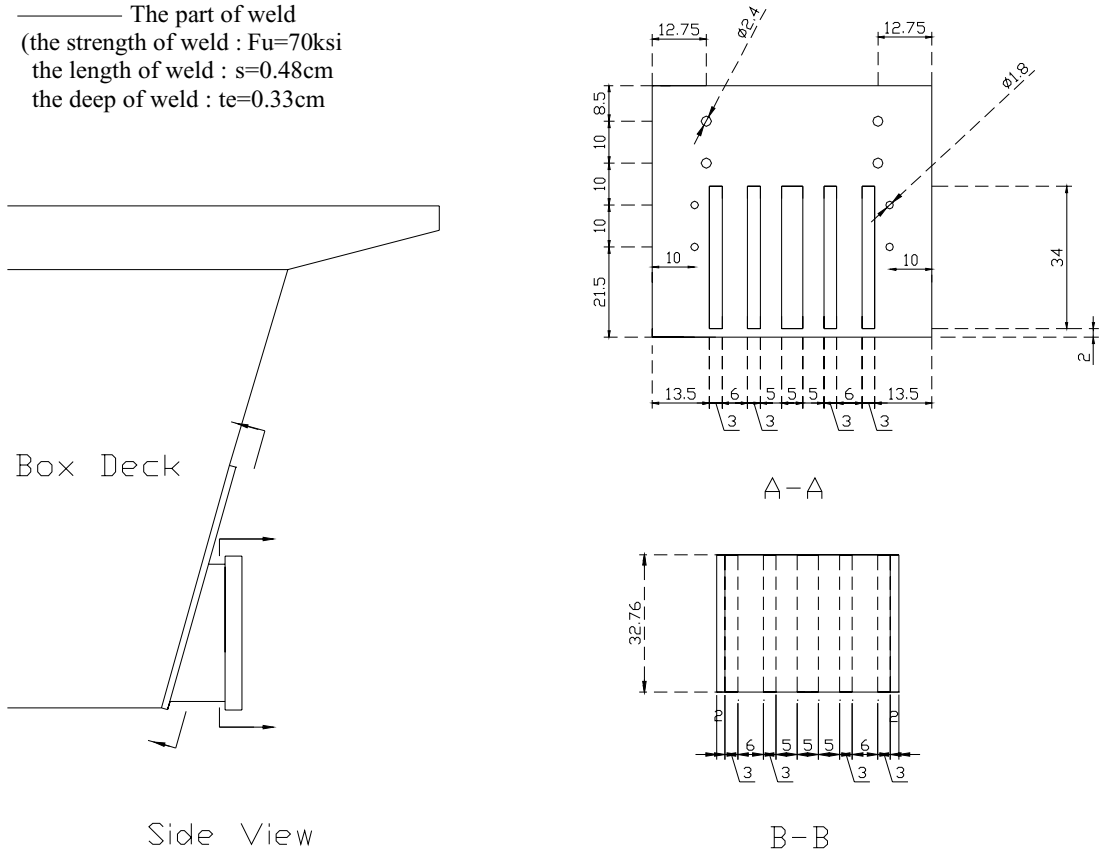

Fig. 32. Detailed design of bearing system.

a. *Position of forces exerted:*
In order to induce the largest displacement possible to the bridges, the forces exerted should be located as close to the middle of the bridge as possible. However, since the bridges lay across the Lion-Head River, the position for the installation of the push-and-fast-released system is limited.
By entering into the box girder, it is inspected that the locations of the diaphragms are right on the top of the piers. The risk of damage will be minimized if forces are exerted just at the position of the diaphragm. It is therefore decided that forces will be exerted to the bridge deck right above the third pier.

b *Installation of instruments:*
Forces are intended to be exerted on the webs of the deck. Since the webs of the box section are inclined, a bearing system with one side of its surface vertical and the other side bolted on the web is designed thereafter (see Fig. 32). Therefore forces induced by the jacks may be exerted on the vertical side of the bearing system and remain horizontal without shifting.
Four steel bars were welded at the edge of the vertical side of the bearing system on the west-bounded bridge to form a rectangular space. The roller end of the hydraulic jack was fixed in position so that the jack is stable. The other end of the jack was bolted on one end of a well-selected wide-flange beam. A semi-sphere steel ball was welded on the other end of the beam. The force induced by the jack will not only be exerted to the deck of the west-bounded bridge, but also be transferred through the beam and the steel ball to the bearing system and the web of the east-bounded bridge.
The jack is equipped with an oil tank which was refitted by the Department of Civil Engineering, National Taiwan University and has the capability of releasing the oil quickly.

Fig. 33. LVDT installed to measure the deformation of LRB.

The whole system was hanged and installed between the decks upon the third piers of the west and east-bounded bridges. Forces induced by the jack pushed the two bridges simultaneously. As the objective force magnitude was reached, the hydraulic oil pressure in the tank was released instantly.

c *Design of the magnitude of force:*
There are several restrictions in the magnitude of the forces exerted. Firstly, the allowable lateral loading of the east-bounded bearing is 134 tons in its original design. To prevent damage to the bearings, the force exerted should be smaller than 134 tons. Secondly, no failure is allowed in the decks during the test.
After a detailed analysis, it is decided that the magnitude of the force should be no more than 90 tons. The jack with a force capacity of 100 tons was thus selected.

d *Design of the structure element*
After the magnitude of the force was decided, the structural elements of the system should be designed and the safety should be insured.
The wide-flange beam is 550 cm in length. Its cross-section was 40 cm $\times$ 40 cm with four stiffeners on each side of the web. Two 44 $\times$ 44 $\times$ 3 cm steel plates were welded at the ends of the beam so that the jack could be bolted on.
The bearing stress in the bearing system under a concentrated load and the shear force along the connection was analyzed by finite element method.
The penetration stress and shear stress in the deck should be analyzed and checked as well. A finite element model was established to check the compression stress of the diaphragm.

5.2. Steps of test

Drilling positions of the bolts that connect the bearing system and the web of the bridge deck are confirmed after the distribution of the steel in the web is known.

Due to the limited number of sensors, the test on the east and west-bounded bridges has to be carried out separately.

Sixteen velocimeters were placed on the deck and on the top of the piers of the west-bounded bridge. Two LVDT were installed at the top of the third pier and at the top of the LRB on that pier, respectively, so as to measure the

Table 4
Displacement, frequencies, and damping ratios of the bridges

	Displacement (mm)		Frequency (Hz)		Damping ratio
	Deck displacement	LRB deformation	From velocity	From LVDT	%
west-bounded bridge	4.35	2.86	2.36	2.35	14.7
	4.33	3.01		2.34	13.1
east-bounded bridge	2.13		3.1	3.12	6.76
	1.98			3.12	6.98

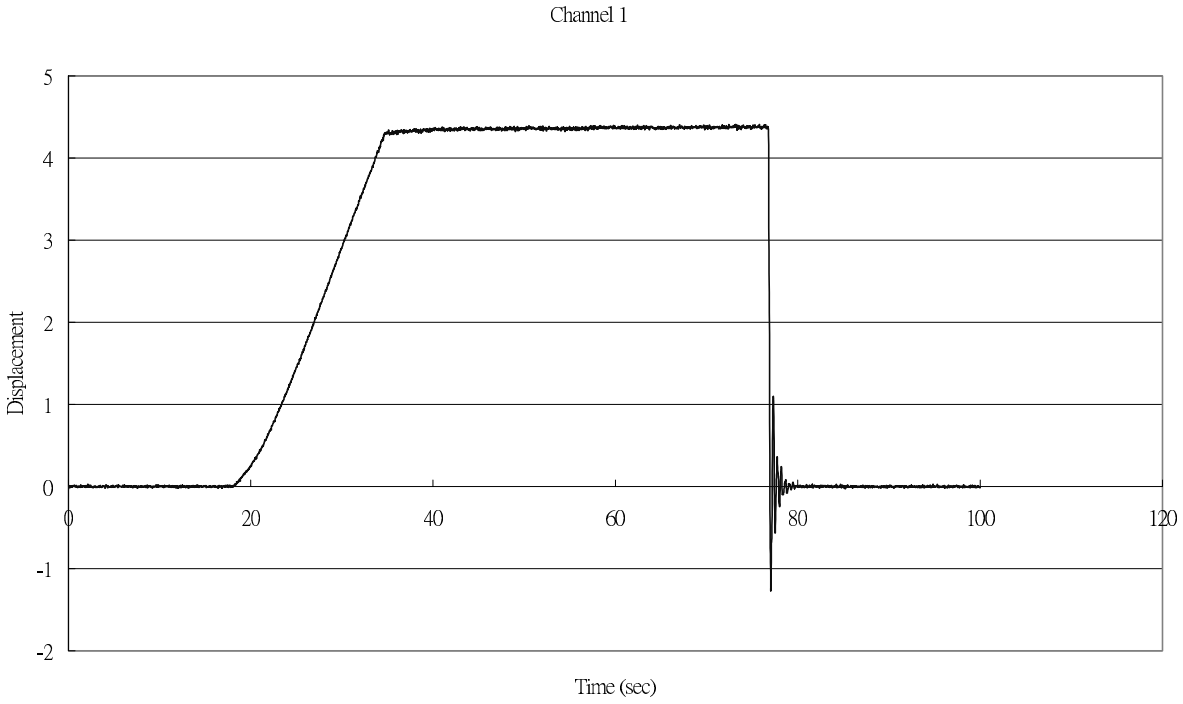

Fig. 34. Displacement of west-bounded bridge in free vibration test.

deformation of LRB (Fig. 33). The other two LVDT were installed beneath the deck at the third and fourth span and a proper distance from the third pier, so as to measure the absolute displacement.

The compressive force induced by the jack was increased slowly. When the force approached 90 tons, the oil in the tank was released quickly. The bridges vibrated freely after their initial displacement.

Repeat the same procedure to the east-bounded bridge, except that the LVDT on the top of LRB is installed on the bottom of the box girder.

It is claimed in literature [9] that variation of ambient temperature may significantly influence the mechanical characteristics of the bearings. Therefore, tests were conducted at noon and in the evening several times for comparing the thermal effect.

5.3. Results

The responses collected from the velocimeters and the LVDT are shown in Figs 34 to 37. Damping ratio of the bridges can be obtained by the logarithmic decrement method. The frequency responses transformed from time domain responses were shown in Figs 38 and 39. The natural frequencies of the bridges are identified. The results are summarized in Table 4.

The initial displacement is mainly in the transverse direction, and so are the frequencies. Comparing with those identified from the other tests, it shows that the frequencies are even lower than that from the force vibration test. This is due to the fact that the response in the free vibration test is the largest.

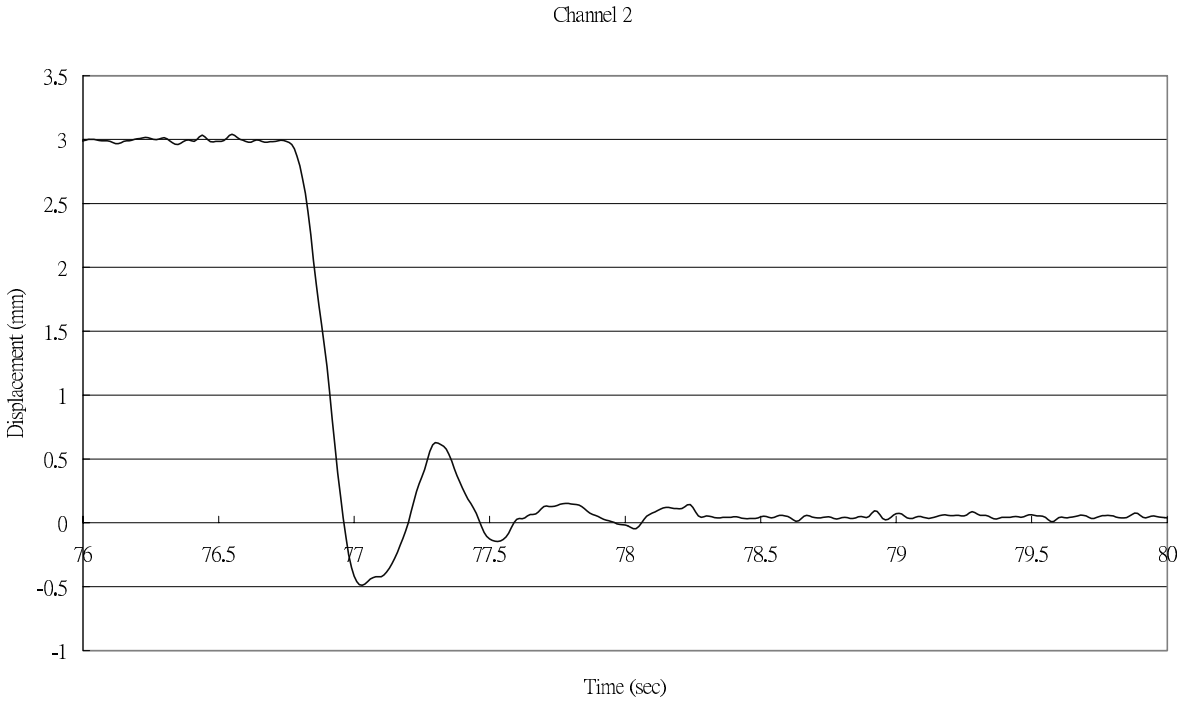

Fig. 35. Deformation of LRB in free vibration test.

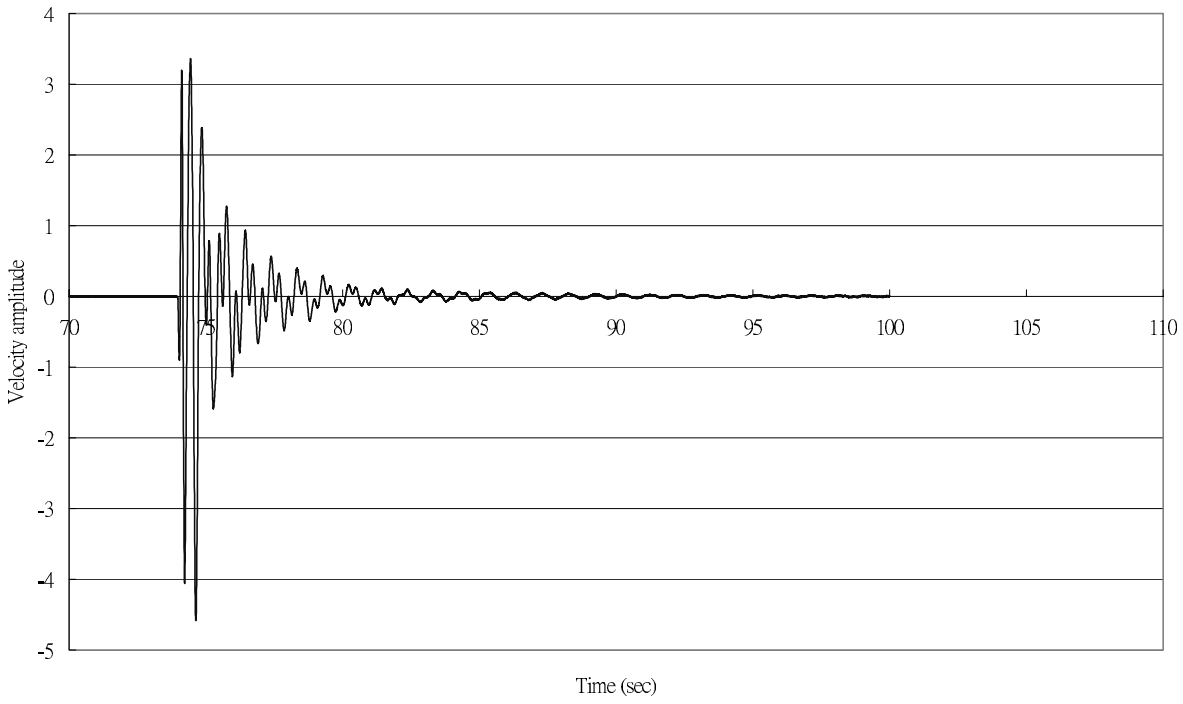

Fig. 36. Velocity of east-bounded bridge in free vibration test.

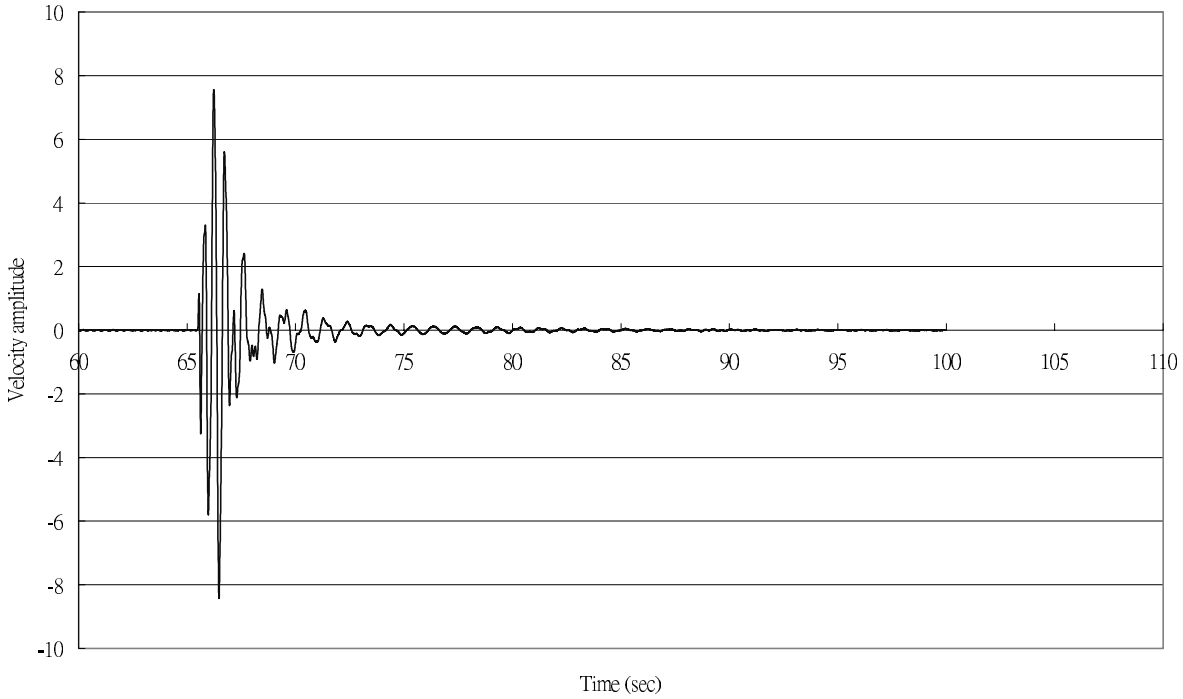

Fig. 37. Velocity of west-bounded bridge in free vibration test.

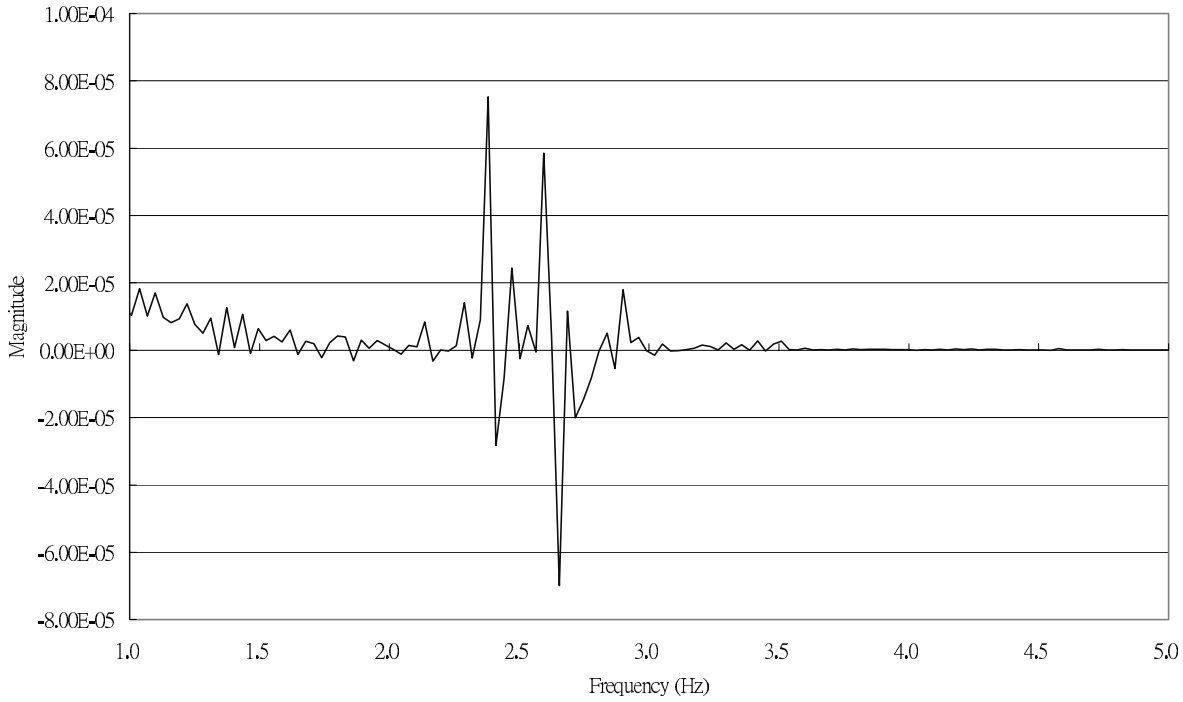

Fig. 38. Frequency response of west-bounded bridge in free vibration test.

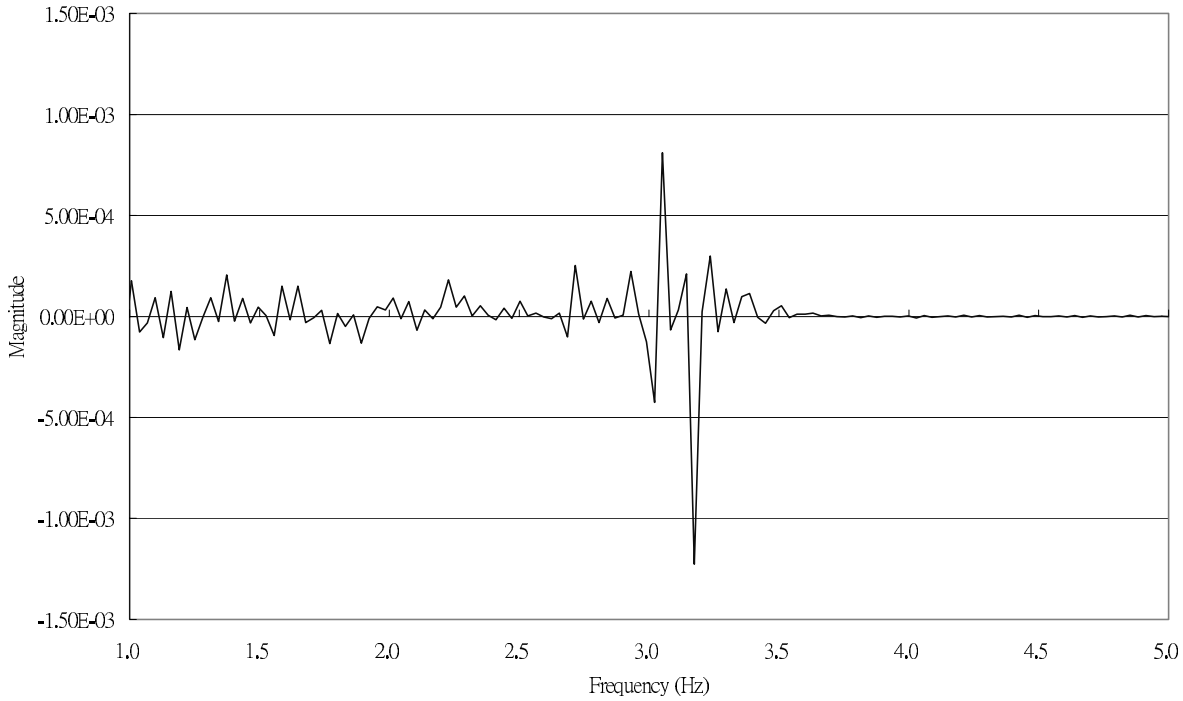

Fig. 39. Frequency response of east-bounded bridge in free vibration test.

The responses of the deck of the west-bounded bridge are mostly contributed from the deformation of the LRB. From the hysteretic characteristics of the LRB, it implies that the more deformed the LRB, the smaller the effective stiffness, and the higher the equivalent damping ratio. Therefore, the damping ratios as well as the period of the west-bounded bridge are larger than those of the east-bounded, and are also larger than those obtained from the other tests.

According to the study in literature [9], the higher the temperature, the smaller the stiffness of the LRB, it is expected that the frequencies identified from the results of the tests conducted at noon will be smaller than those in the evening. However, the difference is not significant in this test. It is probably due to the fact that the thermal difference between noon and in the evening was not large enough at the time of tests. Further, the LRB was installed underneath the bridge deck and was not exposed directly under the sun.

6. Truck test

6.1. Introduction of the test

A two-axle truck with a total weight of 25.34 tons as shown in Fig. 40 was on mission by the contractor to support the test. The stiffness of the suspension system of the truck was measured. The truck was driven to the center of the bridge at a constant speed and then stopped suddenly.

The other tests was to position the rear wheel of the truck on a concrete block on the deck and then move the truck forward and let the wheel drop suddenly from the concrete block and thus induce an impact to the bridge.

6.2. Test result

Vertical velocities of the bridge deck were measured. Responses in frequency domain were obtained through FFT and are shown in Figs 41 and 42. Two major frequencies, i.e., 3.45 Hz and 2.41 Hz, were identified. These frequencies are relevant to the effect of vehicle-bridge interaction and were further investigated in another paper.

Fig. 40. Truck used in the test.

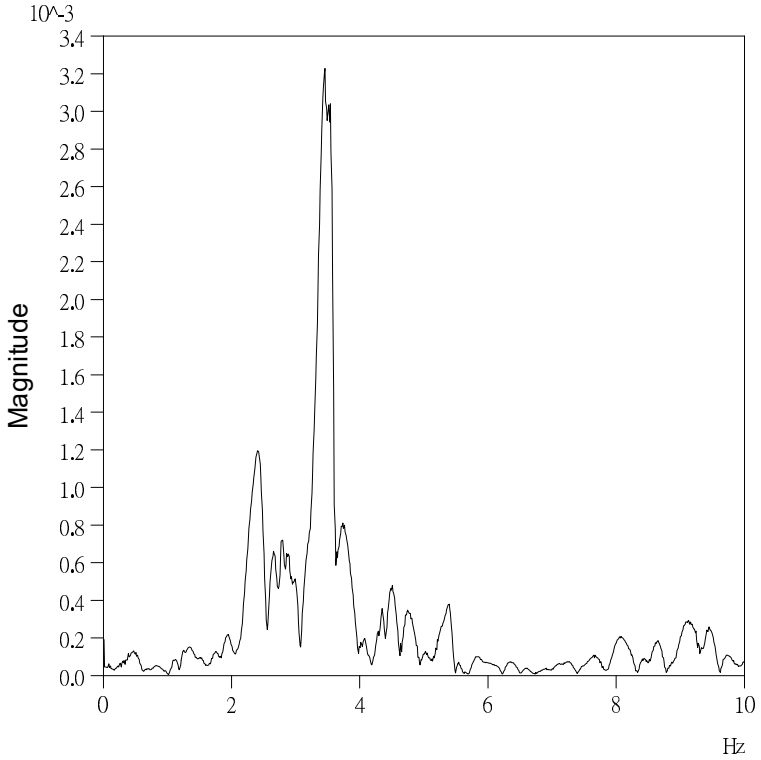

Fig. 41. Frequency response of the east-bounded bridge in the truck test.

Table 5
Impedance functions of soil at PW1 to PW4

	Kz,sur (kN/m)	Ky,sur (kN/m)	Kx,sur (kN/m)	Krx,sur (kN*m)	Kry,sur (kN*m)	Kt,sur (kN*m)
Upper bound	3.959E6	2.616E6	2.616E6	2.785E7	2.777E7	3.224E7
Lower bound	1.188E6	2.354E6	2.616E6	1.706E7	1.427E7	2.355E7

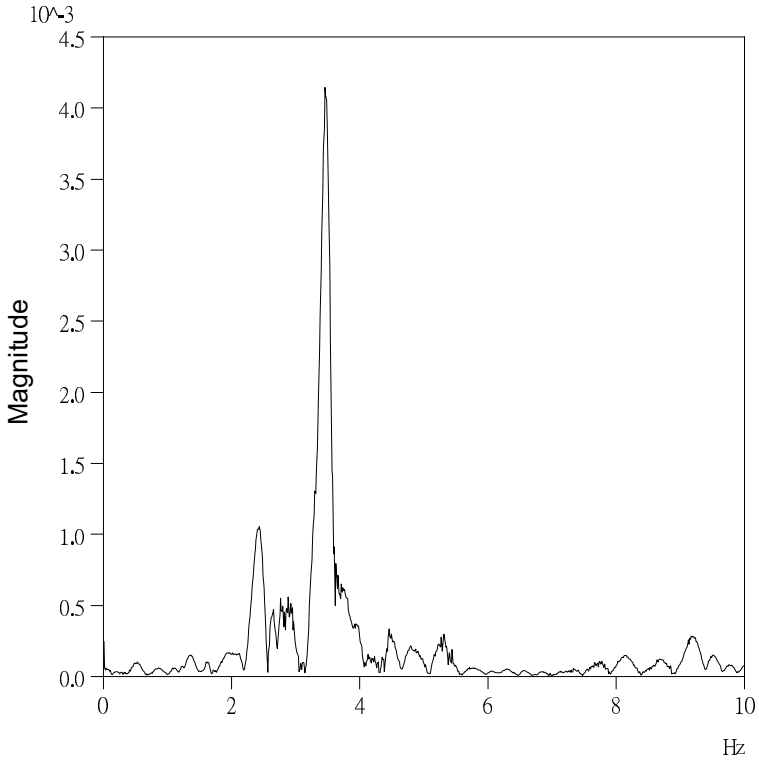

Fig. 42. Frequency response of the west-bounded bridge in the truck test.

However, since the weight of the truck, although carrying the load of New Jersey concrete barriers, is much smaller than that of the bridge, the frequency of 3.45 Hz identified in the test is quite close to the 3.5 Hz-frequency of the bridge identified from the other tests.

7. Theoretical simulation

7.1. Soil-structure interaction

According to the soil properties obtained from geological drilling, and assuming that the ground is a homogeneous half-sphere with an embedded rigid foundation, the impedance functions of soil were evaluated according to the imperial formulas in literature [11].

The impedance functions of soil depend on the excitation frequency. The ranges of the impedance functions at various piers are shown in Tables 5 to 7. Since the bridges are located on hard soil, the upper bounds of the impedance functions were selected in the theoretical simulation.

7.2. Model establishment

SAP2000 software is adopted in the establishment of the bridge model.

Table 6
Impedance functions of soil at PE1 and PE4

	Kz,sur (kN/m)	Ky,sur (kN/m)	Kx,sur (kN/m)	Krx,sur (kN*m)	Kry,sur (kN*m)	Kt,sur (kN*m)
Upper bound	3.615E6	2.349E6	2.407E6	2.579E7	1.884E7	2.503E7
Lower bound	1.085E6	2.349E6	2.166E6	1.241E7	1.147E7	1.819E7

Table 7
Impedance functions of soil at PE2 and PE3

	Kz,sur (kN/m)	Ky,sur (kN/m)	Kx,sur (kN/m)	Krx,sur (kN*m)	Kry,sur (kN*m)	Kt,sur (kN*m)
Upper bound	5.598E6	3.716E6	3.658E6	7.253E7	8.966E7	9.191E7
Lower bound	1.679E6	3.344E6	3.658E6	4.432E7	4.418E7	6.705E7

Table 8
Theoretical frequencies of east-bounded and west-bounded bridges

west-bounded bridge	Frequency (Hz)	Dominate direction
Mode 1	2.4	Transverse
Mode 2	2.38	Longitudinal
Mode 3	3.0	Transverse
Mode 4	3.46	Vertical
Mode 5	4.03	Transverse
Mode 6	4.3	Vertical
Mode 7	5.36	Vertical
east-bounded bridge	**Frequency (Hz)**	**Direction**
Mode 1	3.32	Transverse
Mode 2	3.52	Vertical
Mode 3	3.71	Longitudinal
Mode 4	3.92	Transverse
Mode 5	4.34	Vertical
Mode 6	5.37	Vertical

Based on the hysterestic characteristic of the LRB observed from the experiment, the LRB is modeled as a bilinear element in horizontal direction with initial stiffness $K_1 = 6820$ kgf/cm and post yielding stiffness $K_2 = 545.6$ kgf/cm. Yielding strength $F_y = 42234.4$ kgf and the damping ratio of 29.7% were chosen as well. In addition, it was modeled as linear element with stiffness $K_v = 1000$ ton/cm in the vertical direction.

In the preliminary examination, the vibration frequencies calculated from the models did not match well with that from the experimental testing. This is due to the fact that the superstructure of the bridge is a prestress concrete box girder and the effect of tendons, due to the restriction of the software, was not able to be considered in the model.

It is well known that the effect of tendons in the prestress concrete beam is similar to uniformly distributed upward forces. Therefore, one way to model the tendon effect is to reduce the self weight of the superstructure.

After several iterations, it is suggested that the weights of the east and west-bounded bridges are reduced to 95% and 85%, respectively. Under this circumstance, the frequencies of the bridges are consistent theoretically and experimentally. These revised models are adopted in the following computer simulations.

It is concluded that, in the theoretical modeling, the tendons of the prestress concrete affect the isolated bridge more than the conventional bridge.

The models of east and west-bounded bridges are shown in Fig. 43, theoretical frequencies of the first several modes are shown in Table 8, and the modal shapes of the bridges are shown in Figs 44 and 45.

7.3. Theoretical response of force vibration

We analyzed the responses of the model subjected to sinusoidal forces in X, Y, and Z direction, respectively. The sinusoidal forces were exerted at the position corresponding to where the shakers were installed in the experiment. The frequency of the force varied from 0.5 Hz to 6.0 Hz with an increment of 0.1 Hz.

Fig. 43. Finite element model of the bridge.

As for the velocity at the third span of the bridges, the response in time domain was transformed to frequency domain by FFT. We plotted the frequency responses under various frequencies of sinusoidal excitation on the same graph as shown in Figs 46 to 51.

It is shown that the lower resonance frequencies obtained theoretically are quite close to those obtained experimentally. Since higher resonance frequencies did not show in the experiment so that they cannot be compared with those that are obtained theoretically.

7.4. Theoretical responses of free vibration

We added transverse force at the bottom of the bridge deck above the third pier. The force gradually increased from zero to 90 tons and then was removed. At this time, the initial displacement for the east and west-bounded bridge models is 0.5 mm and 4.4 mm, respectively, as shown in Figs 52 and 53.

The damping ratios are taken into consideration, which were identified in the free vibration test, and the velocity of the third span was analyzed in both time domain and frequency domain, as shown in Figs 54 to 57.

The initial displacement of the west-bounded bridge in the simulation is close to that measured in the experiment, but that of the east-bounded simulated is smaller than observed. This is probably due to the reason that the frame set up between the two bridges was used as the datum in measuring the displacements, and the vibrations in the push-and-fast-release test made measuring the displacement of decks not accurate.

The simulated frequency matched with that obtained experimentally for the east-bounded bridge. However, the simulated frequency is smaller than that obtained experimentally for the west-bounded bridge. This is due to the reason that the effectiveness of stiffness of the LRB is adopted in the theoretical analysis, not the hysteretic characteristic.

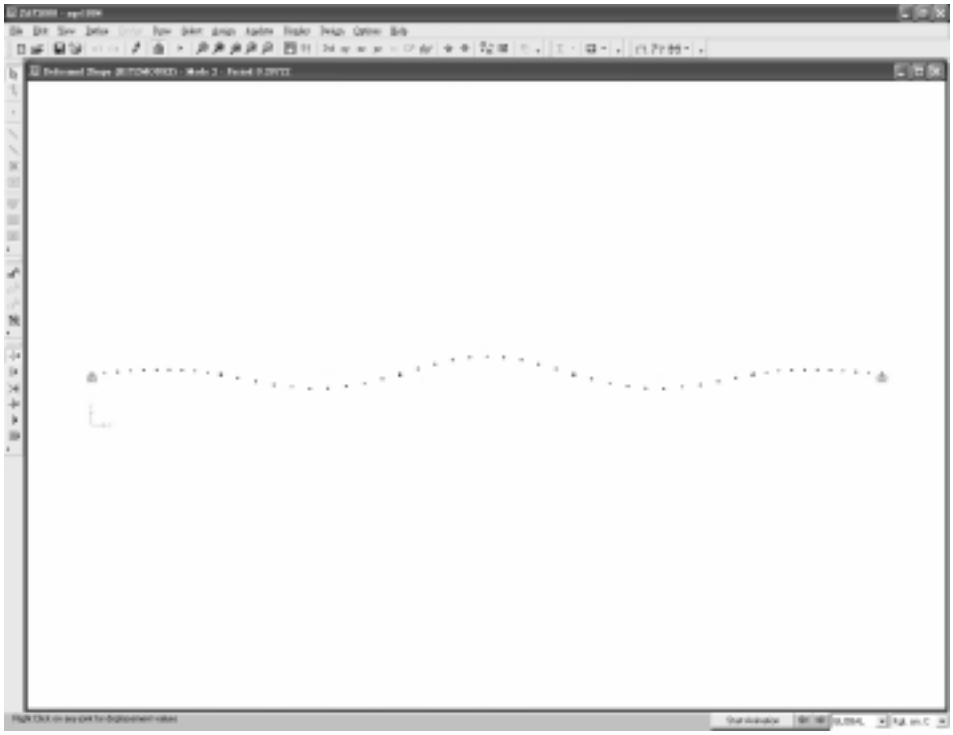

Fig. 44. Mode shape (in vertical direction) of the east-bounded bridge.

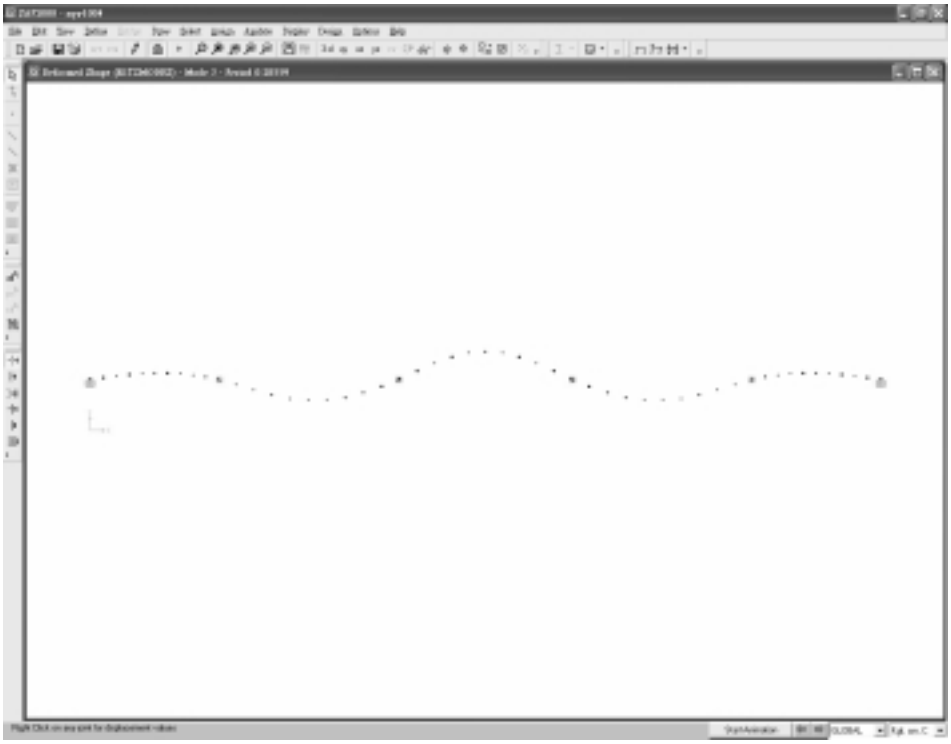

Fig. 45. Mode shape (in vertical direction) of the west-bounded bridge.

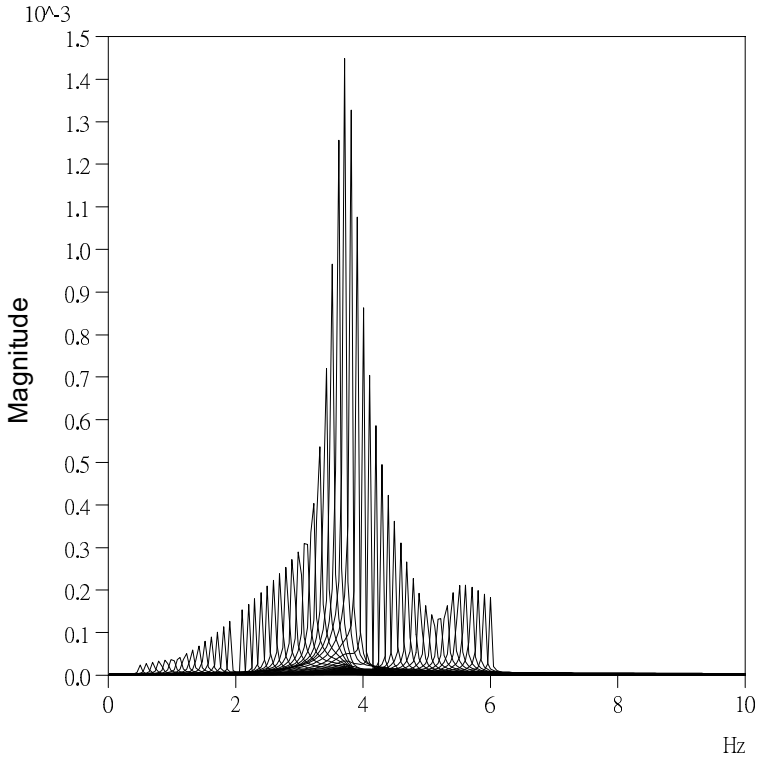

Fig. 46. Theoretical frequency responses in longitudinal direction of the east-bounded bridge under force vibration test.

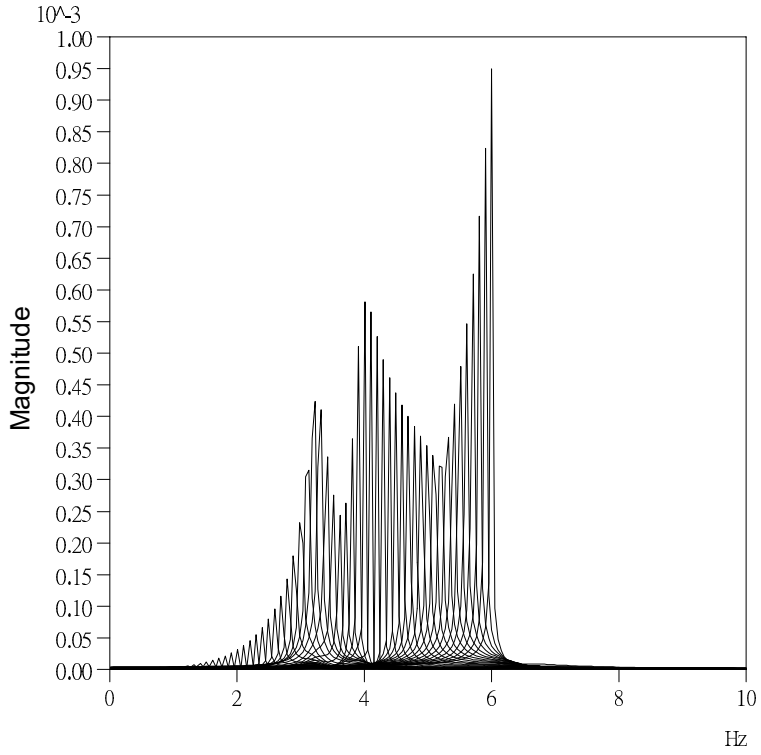

Fig. 47. Theoretical frequency responses in transverse direction of the east-bounded bridge under force vibration test.

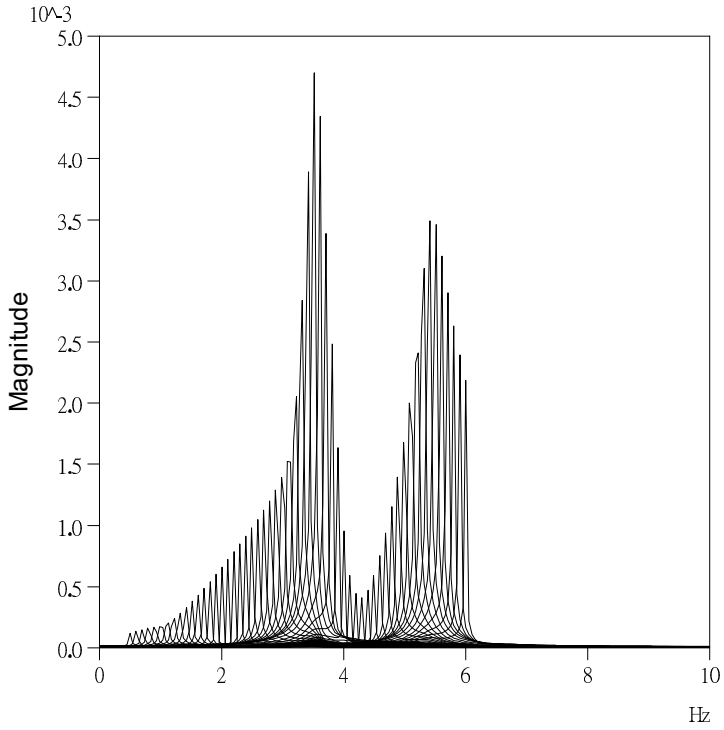

Fig. 48. Theoretical frequency responses in vertical direction of the east-bounded bridge under force vibration test.

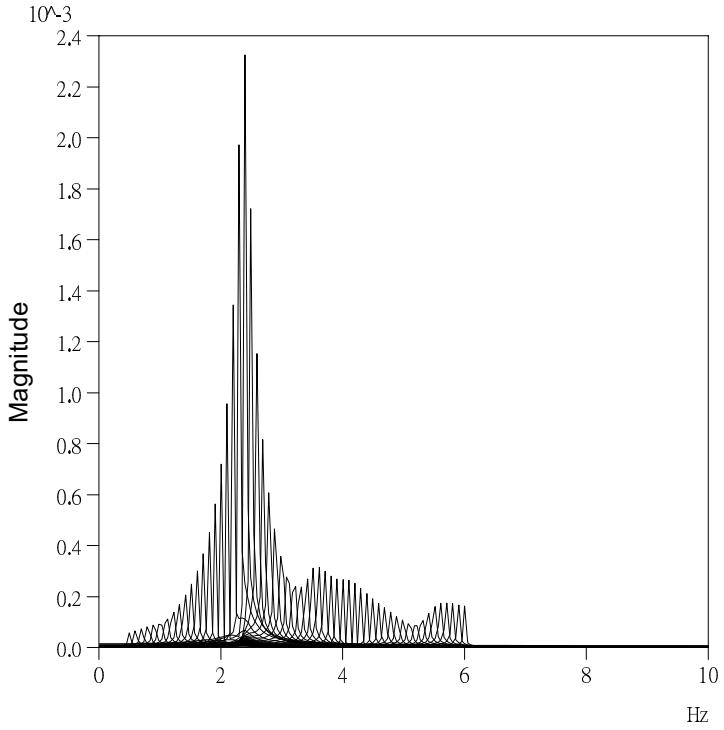

Fig. 49. Theoretical frequency responses in longitudinal direction of west-bounded bridge under force vibration test.

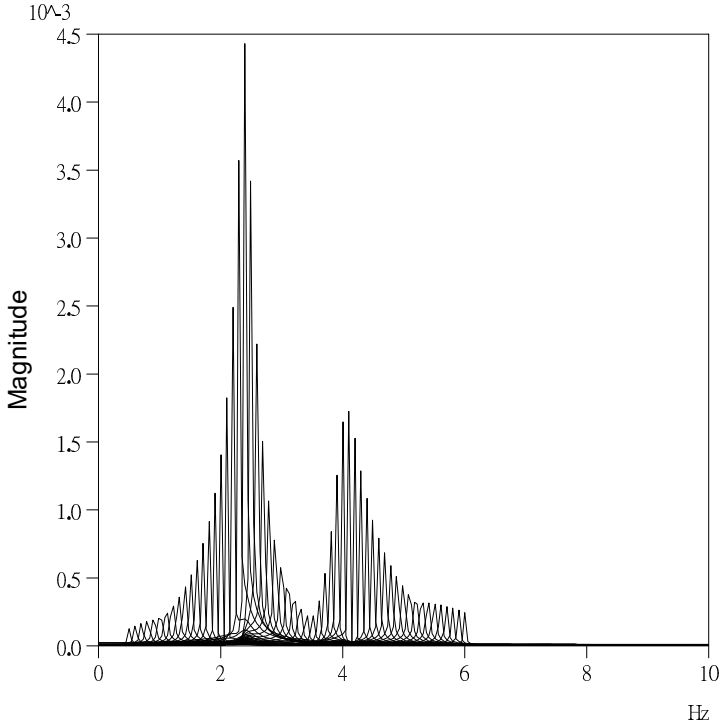

Fig. 50. Theoretical frequency responses in transverse direction of west-bounded bridge under force vibration test.

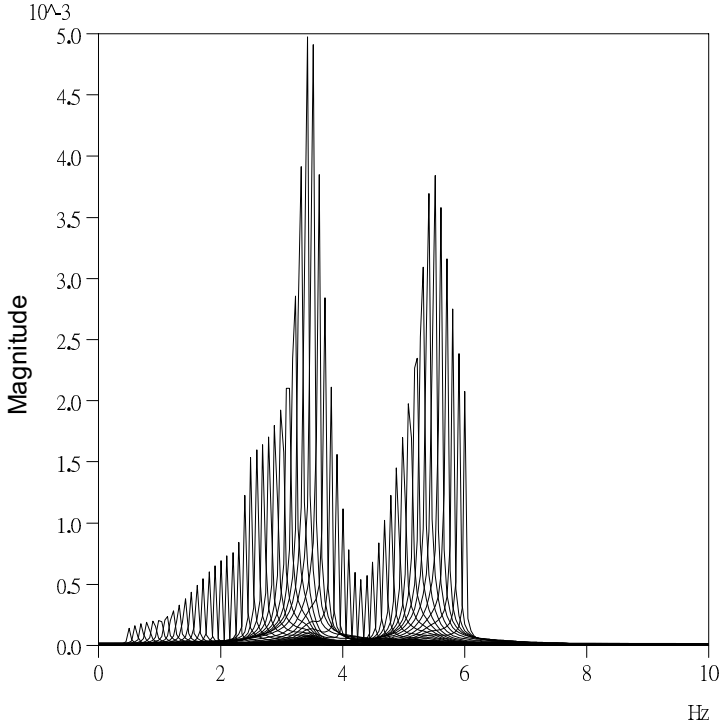

Fig. 51. Theoretical frequency response in vertical direction of west-bounded bridge under force vibration test.

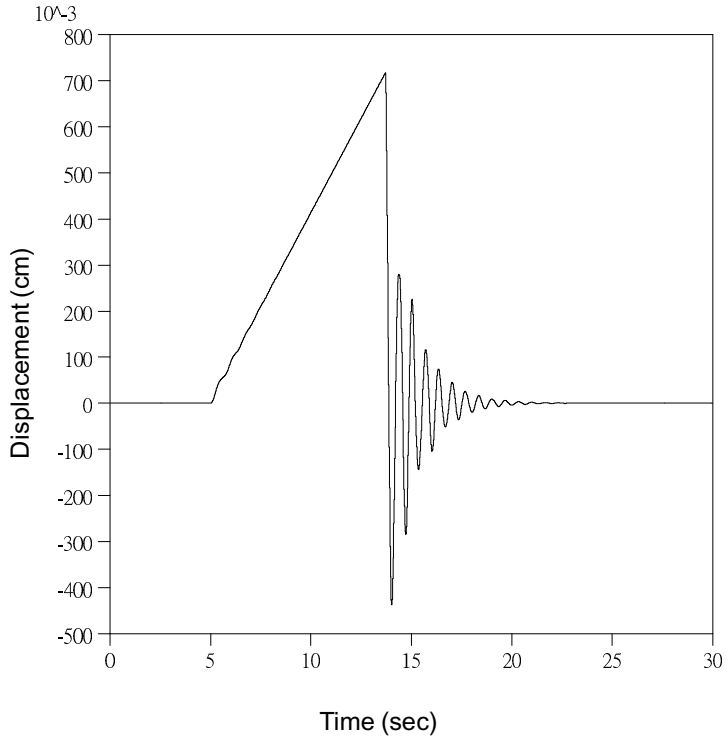

Fig. 52. Theoretical displacement on the deck of the west-bounded bridge under free vibration.

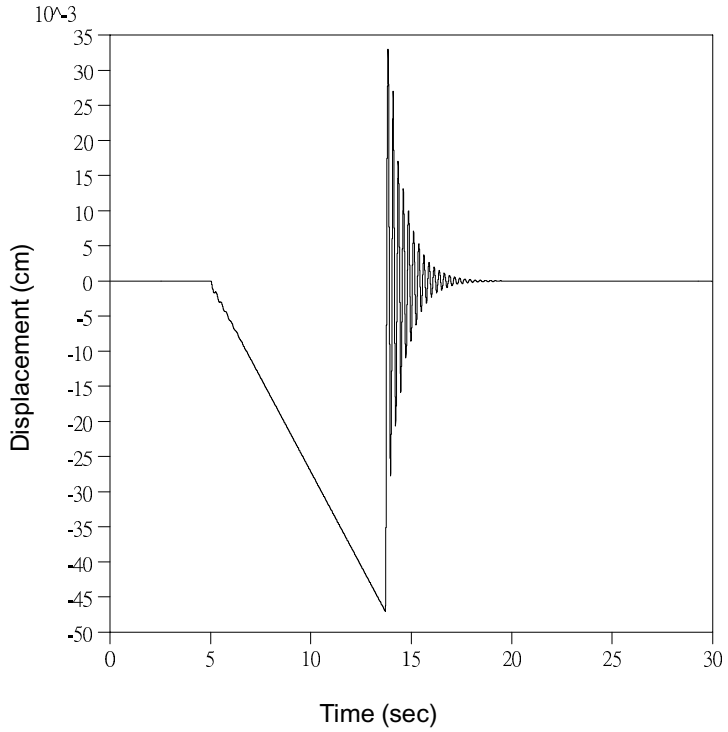

Fig. 53. Theoretical displacement on the deck of the east-bounded bridge under free vibration.

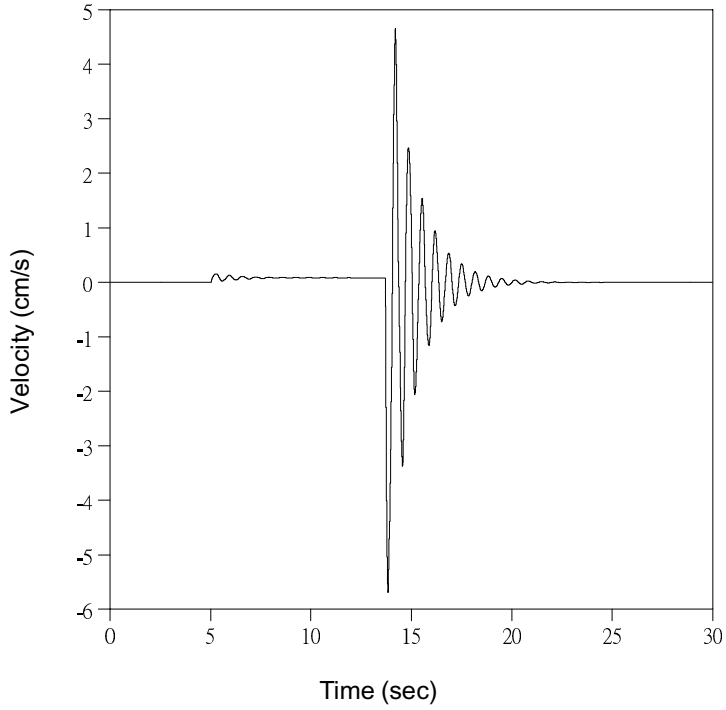

Fig. 54. Theoretical velocity on the deck of the west-bounded bridge under free vibration.

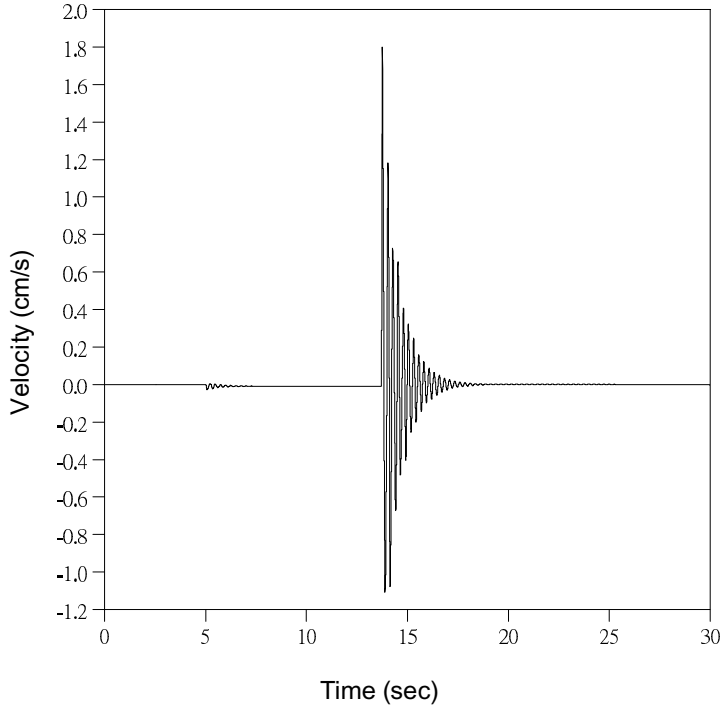

Fig. 55. Theoretical velocity on the deck of the east-bounded bridge under free vibration test.

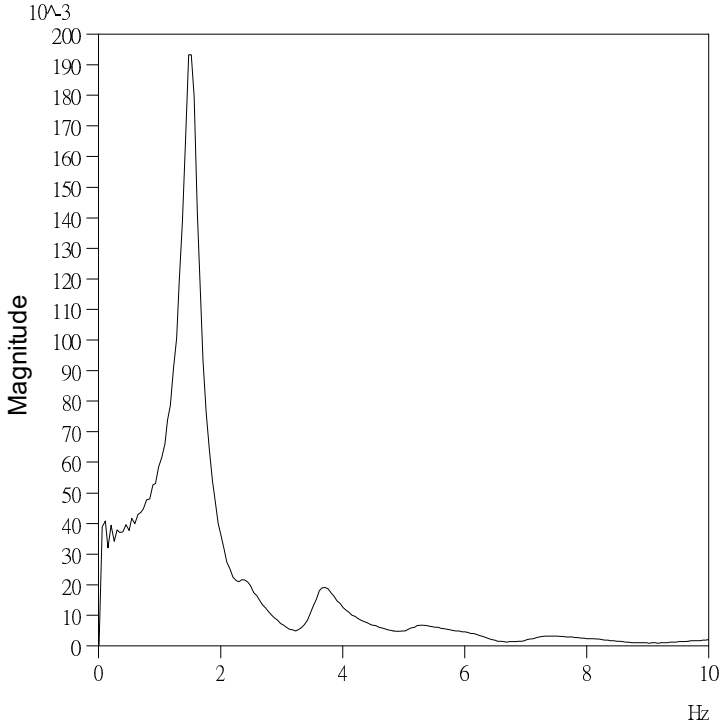

Fig. 56. Theoretical frequency response of the west-bounded bridge under free vibration.

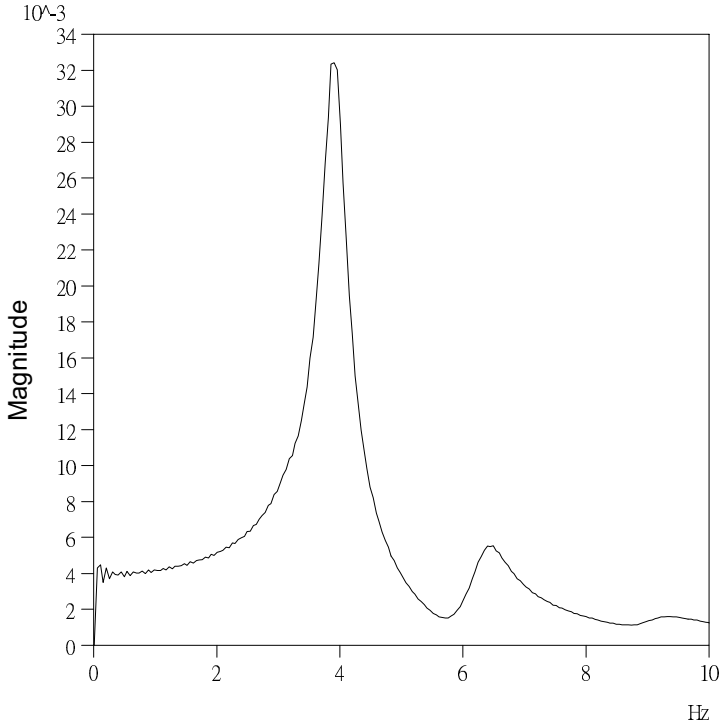

Fig. 57. Theoretical frequency response of the east-bounded bridge under free vibration.

Table 9
Comparison of accelerations between east-bounded and west-bounded bridges under Chia-I earthquake

Case1		east-bounded	west-bounded	Reduction%
CHY035	Acceleration (x)	446gal	213gal	52.2
	Acceleration (y)	1026gal	678gal	33.9
	Acceleration (z)	429gal	291gal	32.2
Case2		east-bounded	west-bounded	Reduction%
CHY035 (2 times)	Acceleration (x)	891gal	407gal	54.3
	Acceleration (y)	2052gal	1232gal	40.0
	Acceleration (z)	858gal	581gal	32.3

7.5. Simulation of the truck test

An impulsive force as shown in Fig. 58 was used to simulate the impact induced by the truck falling from the concrete block to the bridge. The displacements of the east and west-bounded bridges are analyzed and shown in Figs 59 and 60. The maximum displacements for the east and west-bounded bridges are 0.093 cm and 0.103 cm, respectively. Responses in frequency domain are also obtained by FFT after revising the baseline in time domain and are shown in Figs 61 and 62.

The frequencies for the first and second simulated modes are 3.45 and 5.45 Hz, respectively. The simulated 3.45 Hz is the same as that obtained in the truck test.

On the other hand, as a static force is applied to the model, it is found that the maximum displacements for the east and west-bounded bridge models are 0.069 cm and 0.076 cm, respectively. Comparing them with the maximum displacements in the preceding paragraph, it is shown that the impact factor of 1.3 is quite reasonable as suggested by many bridge design codes.

7.6. Responses under the Chia-I earthquake

To compare the seismic protection efficiency of the isolated system, responses of the bridge models under a specific seismic excitation is analyzed.

There is a strong motion permanent network installed in Taiwan by the Central Weather Bureau that can collect the seismic signals at many locations. The station that is closest to the bridge site is Station CHY035. The seismic acceleration collected at this station during the Chia-I earthquake (October 22, 1999) is adopted in this analysis. Its maximum acceleration in E-W, N-S, and vertical directions is 438.0, 260.3, and 131.2 gal, respectively, as shown in Fig. 63.

Analytical responses of the bridge deck for east and west-bounded bridges under this excitation are compared in Figs 64 to 66. The hysteretic loop of the LRB is shown in Fig. 67.

It is noted that, the accelerations of the west-bounded bridge in three directions are smaller than those of the east-bounded bridge. The responses can be reduced about 30% due to isolation as shown in Table 9.

The isolation effect can be verified by examining the acceleration spectrum of this excitation as shown in Fig. 68. It is evident that the natural period of the west-bounded bridge is farther away from the dominant period of the earthquake than that of the east-bounded bridge. Therefore the response of the west-bounded bridge will be smaller than that of the east-bounded bridge.

We multiplied the acceleration records at station CHY035 by two and then analyzed the response of the bridges again. The maximum accelerations of the deck were compared with that obtained in the previous paragraph and was also summarized in Table 9. It is shown that the reduction efficiency for the isolation system is increased when the excitation is larger. This is due to the fact that more energy is dissipated by the hysteretic loop of the LRB as can be seen in Fig. 69.

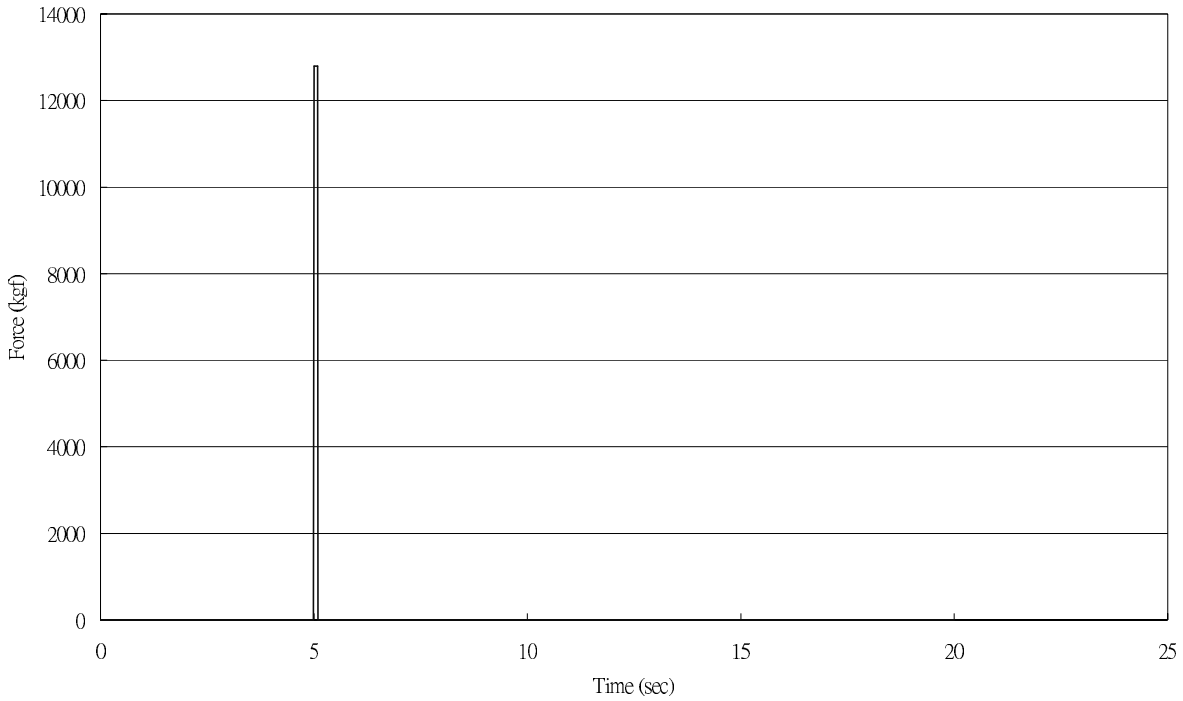

Fig. 58. Impulsive force in the truck test.

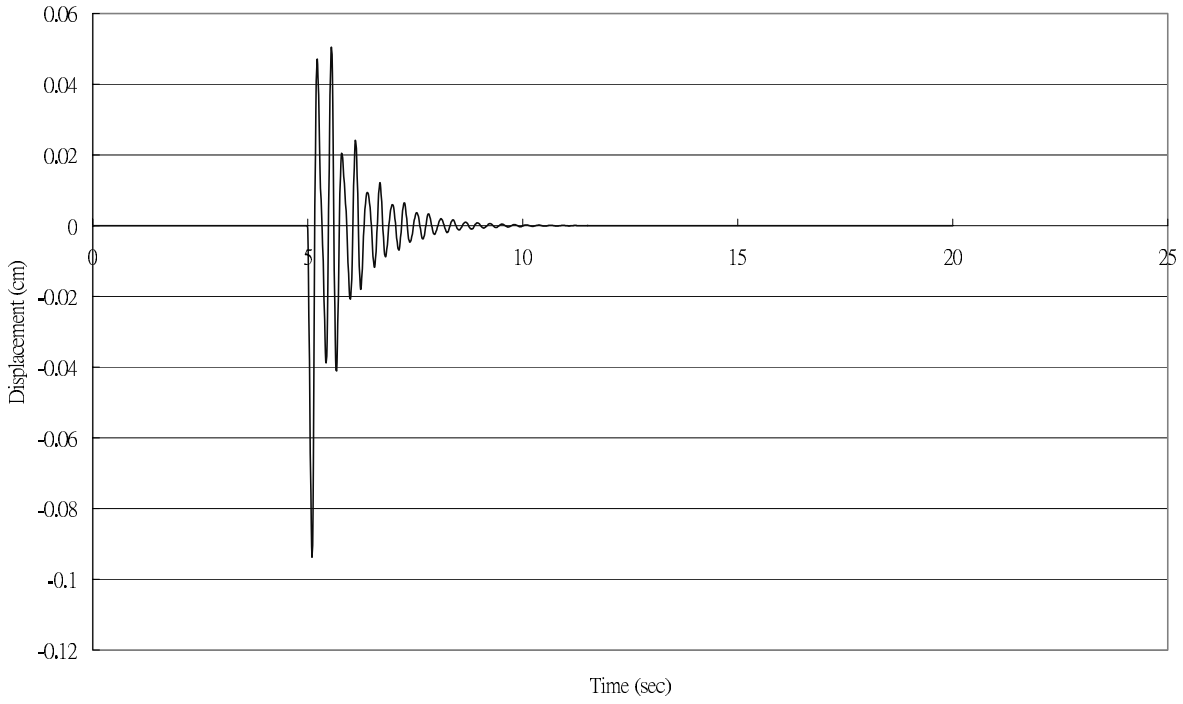

Fig. 59. Theoretical displacement of the east-bounded bridge in the truck test.

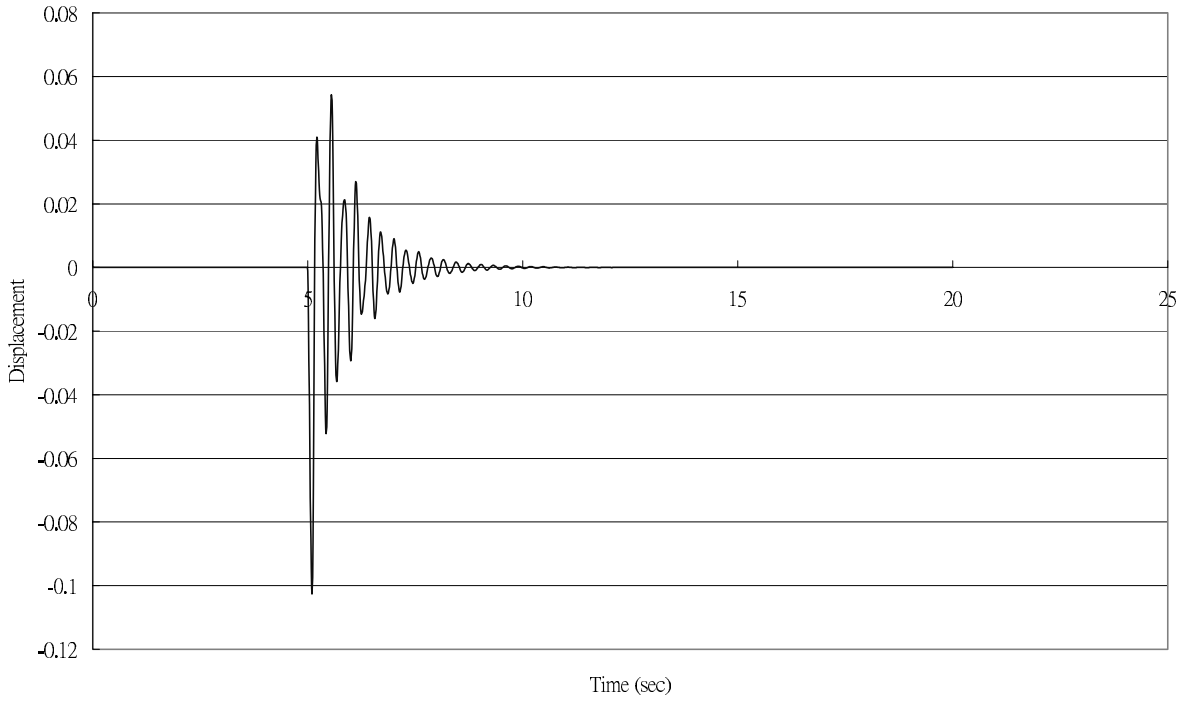

Fig. 60. Theoretical displacement of the west-bounded bridge in the truck test.

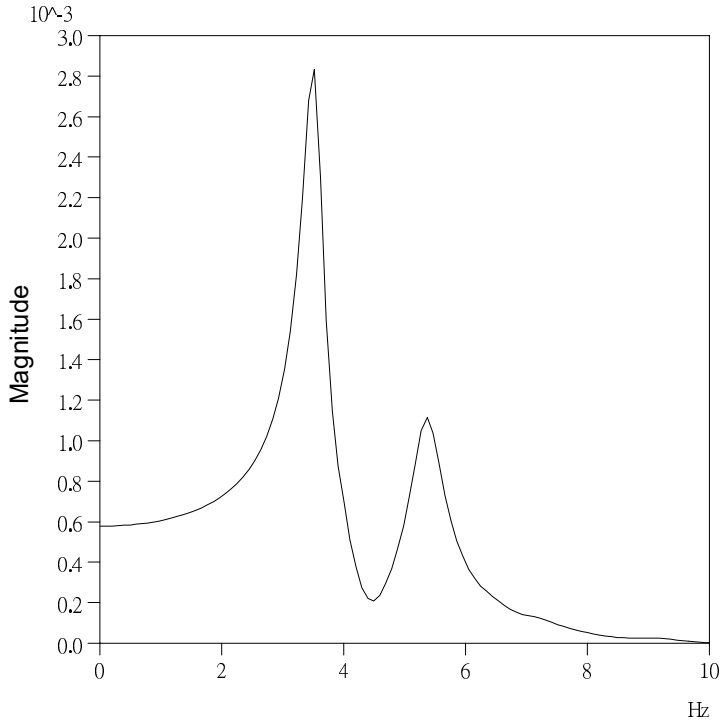

Fig. 61. Theoretical frequency response of the east-bounded bridge in the truck test.

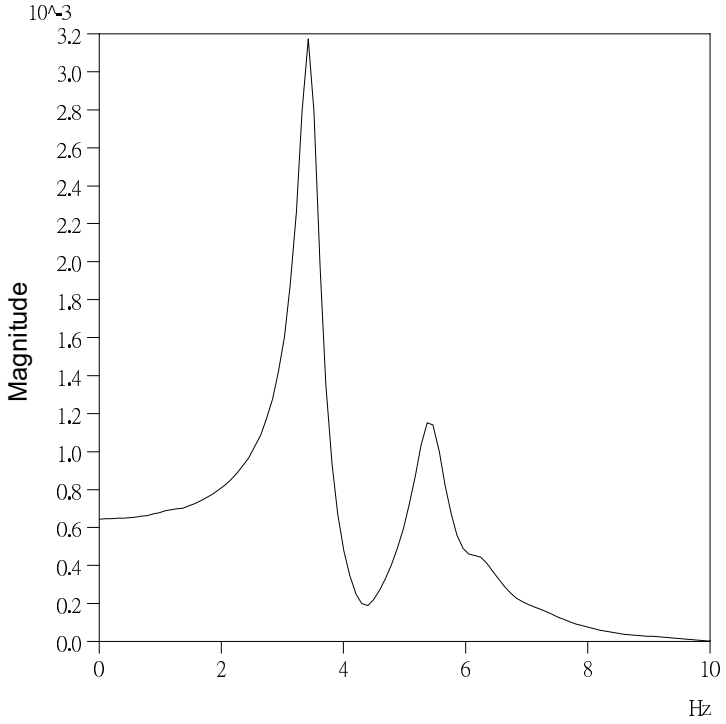

Fig. 62. Theoretical frequency response of the west-bounded bridge in the truck test.

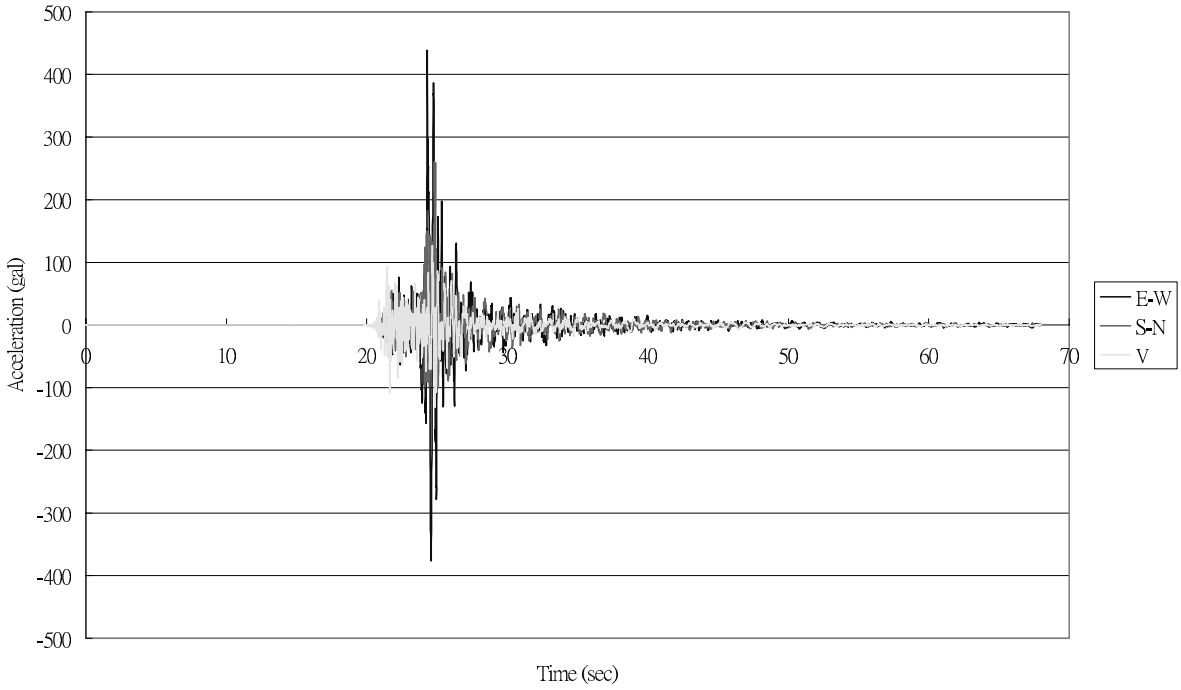

Fig. 63. Acceleration of Chia-I earthquake at Station CHY035.

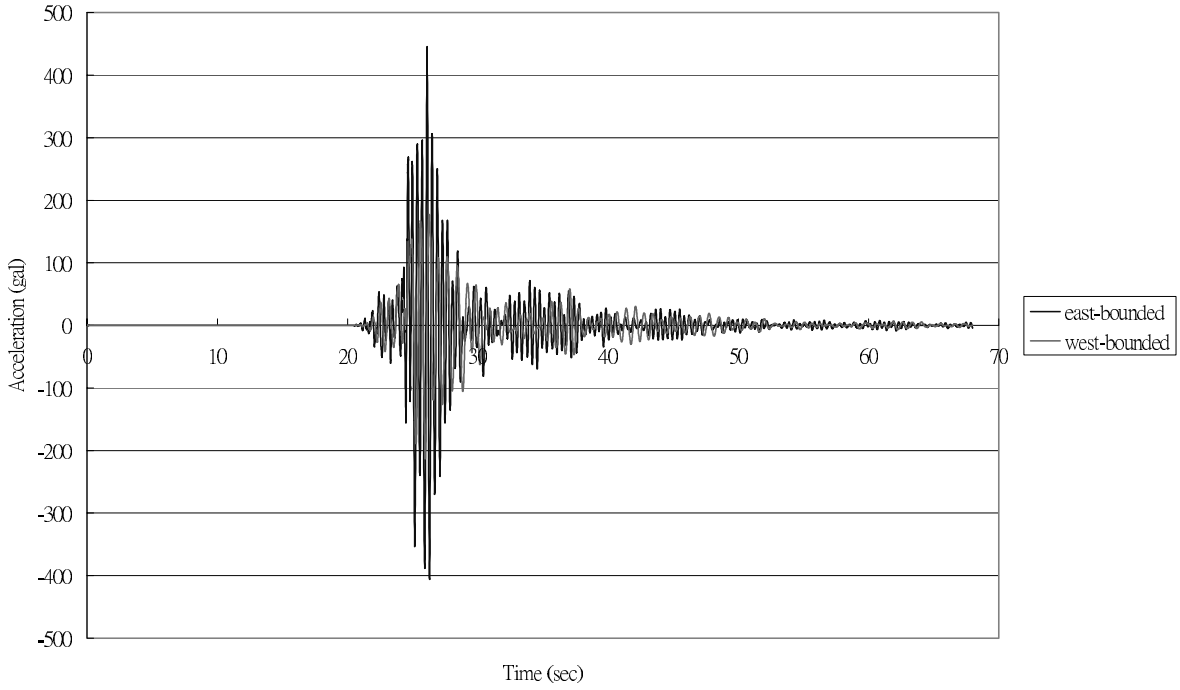

Fig. 64. Acceleration compared between east-bounded and west-bounded bridges in longitudinal direction.

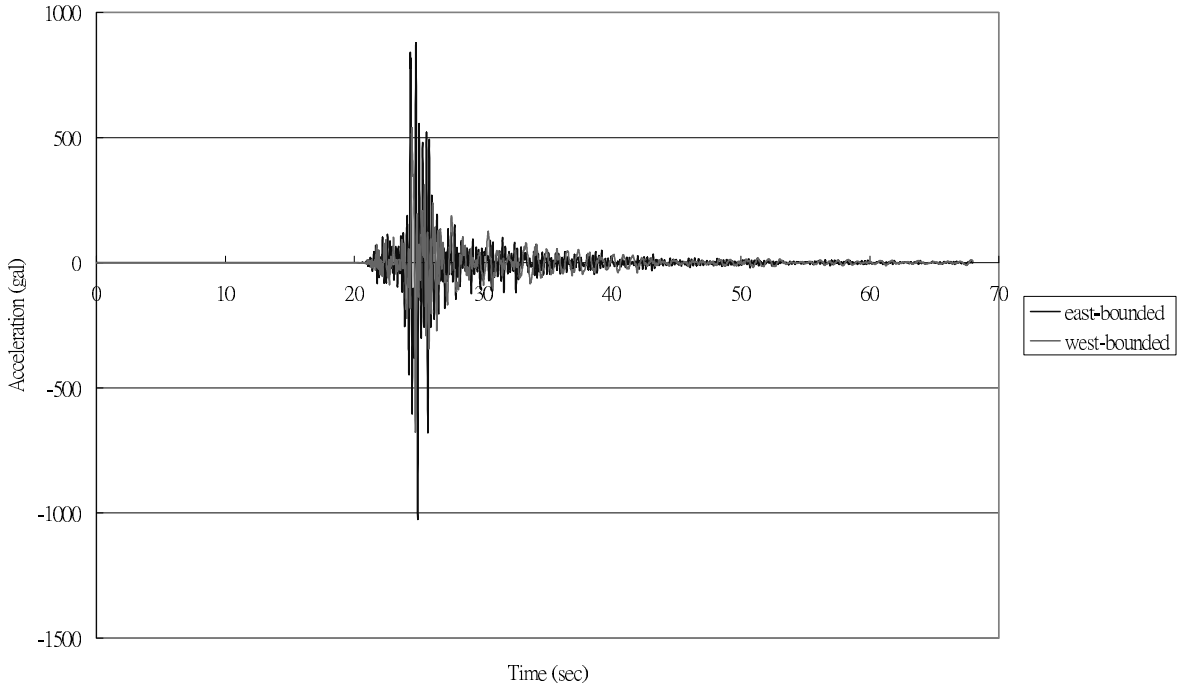

Fig. 65. Acceleration compared between east-bounded and west-bounded bridges in transverse direction.

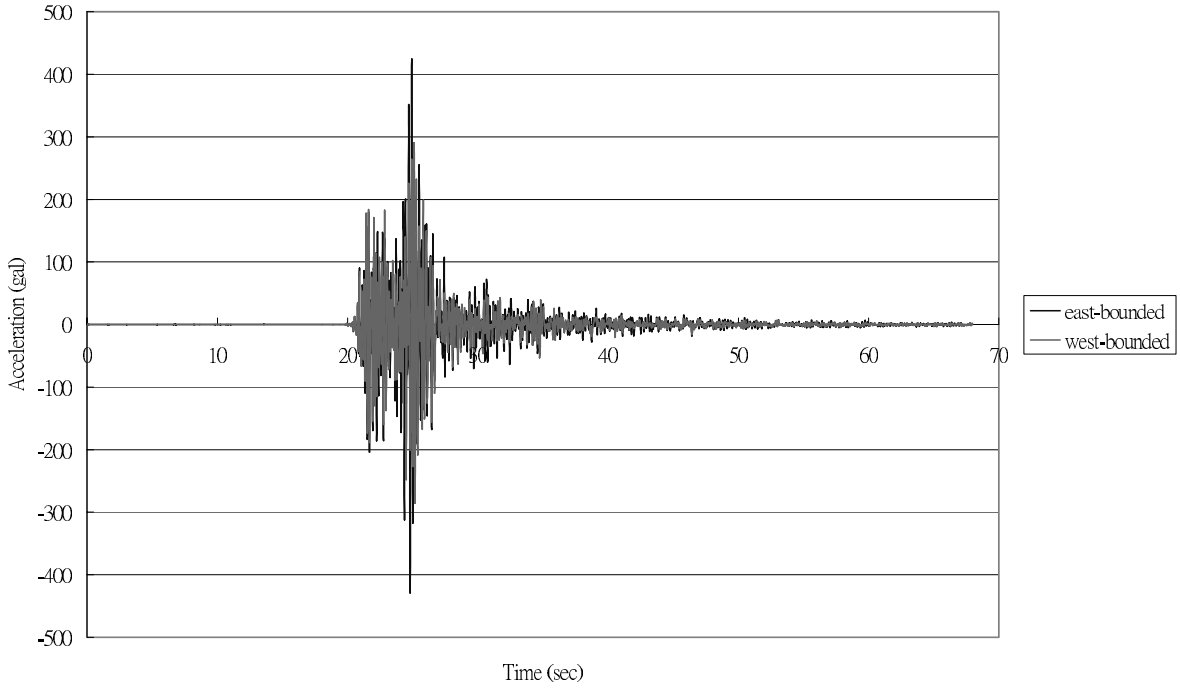

Fig. 66. Acceleration compared between east-bounded and west-bounded bridges in the vertical direction.

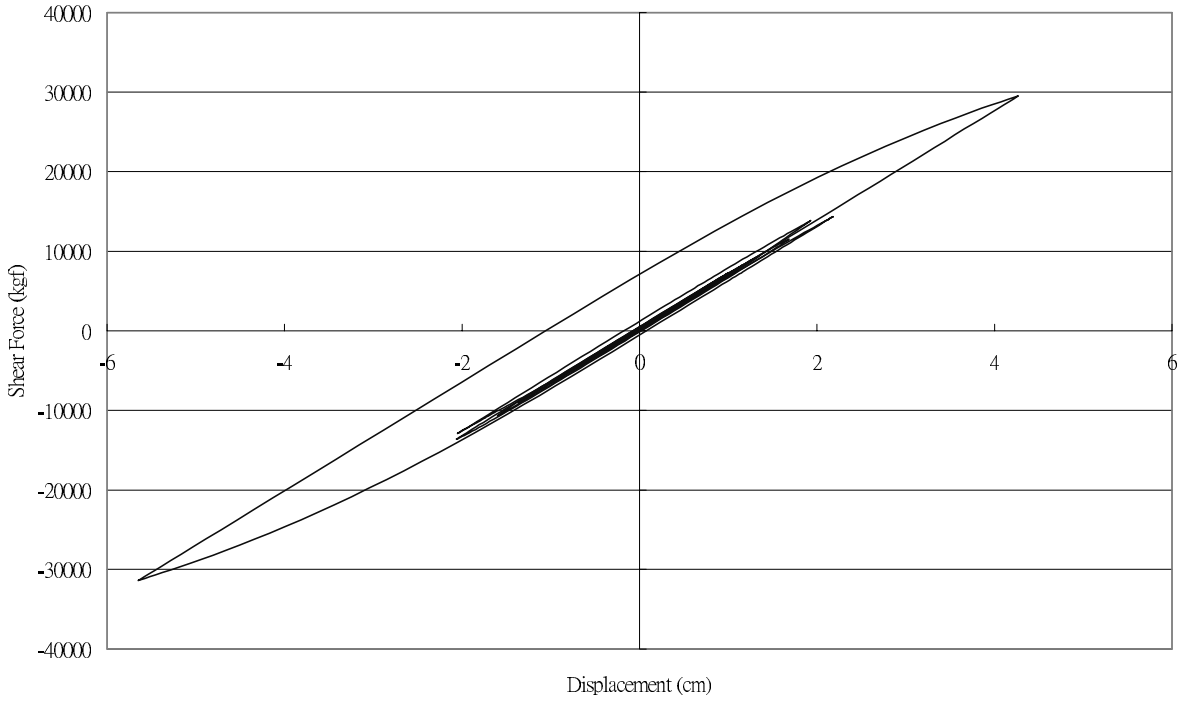

Fig. 67. Hysteretic loop of lead rubber bearing during Chia-I earthquake.

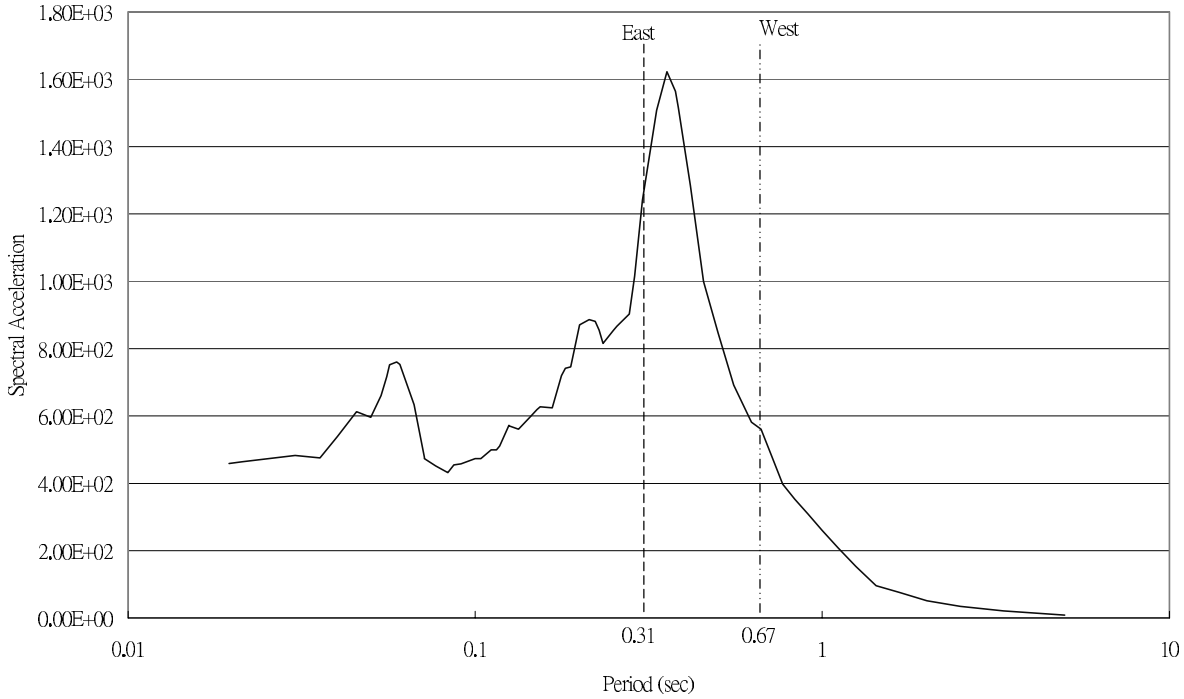

Fig. 68. Spectral acceleration in the transverse direction of Chia-I earthquake.

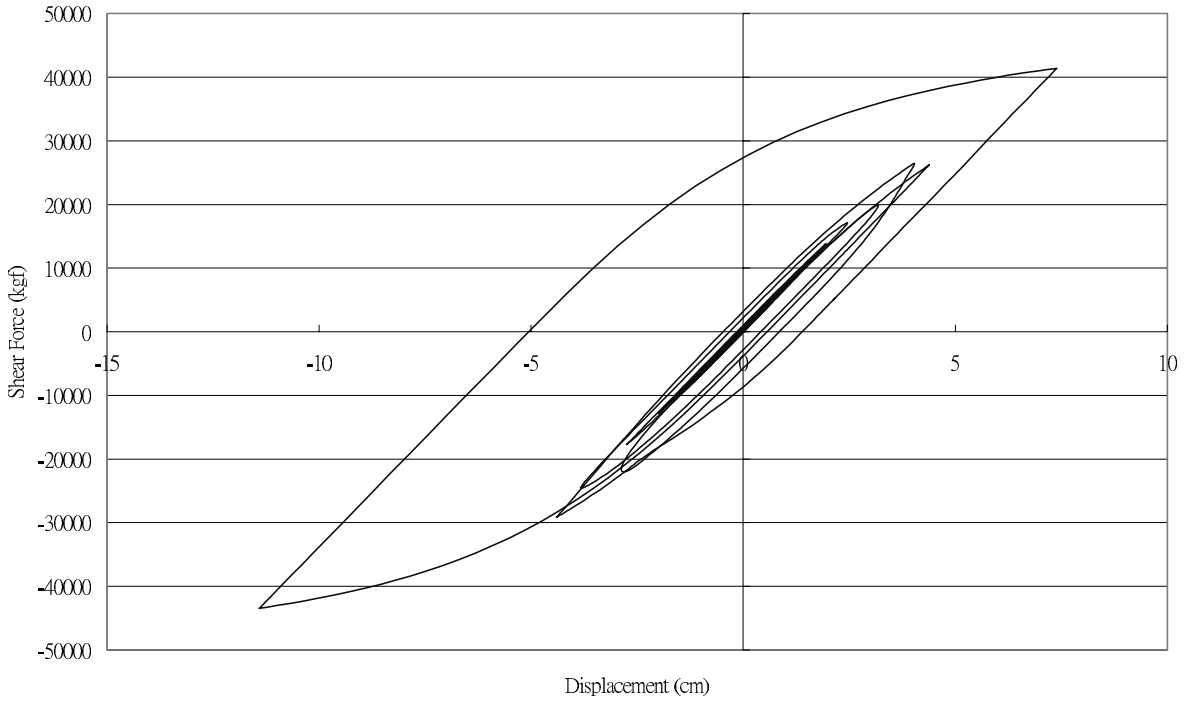

Fig. 69. Hysteretic loop of lead rubber bearing under two times the Chia-I earthquake.

Table 10
Comparison of frequencies among theoretical and various field tests (Hz)

	west-bounded bridge			east-bounded bridge		
	Longitudinal	Transverse	Vertical	Longitudinal	Transverse	Vertical
ambient vibration	2.52	2.7	3.51	3.93	3.23	3.51
Force vibration	2.3	2.5	3.5	3.7	3.2	3.5
Free vibration		2.35			3.12	
Truck test			3.45			3.45
Theoretical	2.38	2.4	3.46	3.71	3.32	3.52

8. Conclusion

1. Dynamic behavior of bridges can be obtained by a series of field tests. The Lion-Head River Bridge, during its construction stage, was processed by several types of tests, including an ambient vibration test, a force vibration test, a free vibration test and a truck test. The ambient vibration test can detect the natural frequency of bridges in three directions. The forced vibration test can detect the vibration frequency, the damping ratio and the vibration modes. A free vibration test is able to detect the frequency, the damping ratio and the vibration mode in transverse direction.
2. Comparisons of the results among an ambient vibration test, a forced vibration test and a free vibration test are shown in Table 10. The frequency obtained from an ambient vibration test is the highest, and that from the free vibration test is the lowest. It is shown that, in the field tests, the larger the response of the structure, the smaller the frequency identified. The variation of frequencies is more obvious for the west-bounded bridge than for the east-bounded bridge. This is due to the fact that the larger the LRB deformed, the less its effective stiffness.
3. The bridges underwent the Chi-Chi earthquakes and Chia-I earthquake during the construction stage. Pot bearings on PE1 and the abutment of the east-bounded bridge were damaged. However for the west-bounded bridge, only conventional rubber bearings on the abutments were damaged. It is demonstrated that the LRB of an isolated bridge has a better aseismic performance than the conventional bearings.
4. From the ambient vibration test, the variation of frequencies before and after the bridge was damaged, and after retrofitted, can be identified. The damage may be reflected in the changes of the natural frequencies. This implies the possible application of a bridge health monitor.
5. Theoretical models are established. The analytical responses of the bridges are quite close to those obtained experimentally. Based on these models, theoretical analysis shows that an isolated bridge has a better aseimic protection efficiency than a conventional bridge.

Acknowledgements

The research was partly supported by the National Science Council, R.O.C. through grant no. NSC91-2211-E-035-019 and is gratefully acknowledged. Financial support from Taiwan Area National Expressway Engineering Bureau, and the Sinotech Engineering Consultant Ltd., and assistance from the National Center for Research on Earthquake Engineering, and Department of Civil Engineering, Taiwan University are deeply appreciated.

References

[1] C.S. Huang and H.L. Lin, Modal identification of structures from ambient vibration, free vibration, and seismic response data via a subspace approach, *Earthquake Engineering and Structural Dynamics* **30** (2001), 1857–1878.
[2] C.R. Farrar and G.H. James III, System identification from ambient vibration measurement on a bridge, *Journal of Sound and Vibration* **205**(1) (1997), 1–18.
[3] A.A. Shama, J.B. Mander, S.S. Chen and A.J. Aref, Ambient vibration and seismic evaluation of a cantilever truss, *Engineering Structure* **23** (2001), 1281–1292.
[4] Eric Abrahamson Seismic response modification device elements for bridge structures development and verification, *Computers and Structures* **81** (2003), 463–467.

[5] R.L. Boroschek, M.O. Moroni and M. Sarrazin, Dynamic characteristics of a long span seismic isolated bridge, *Engineering Structure* **25** (2003), 1479–1490.
[6] Q. Chen, B.M. Douglas, E.A. Maragakis and I.G. Buckle, Extraction of hysteretic properties of seismically isolated bridge from quick-release field tests, *Earthquake Engineering and Structural Dynamics* **31** (2002), 333–351.
[7] H. Kaplan and A. Seireg, A base isolation system for bridges subjected to seismic disturbances, *Earthquake Engineering and Structural Dynamics* **31** (2002), 1093–1112.
[8] J.S. Hwang and T.Y. Hsu, A fractional derivative model to include effect of ambient temperature on HDR bearings, *Engineering Structure* **23** (2001), 484–490.
[9] L. Fryba and M. Pirner, Load tests and modal analysis of bridge, *Engineering Structure* **23** (2001), 102–109.
[10] R. Johansson, *System Modeling and Identification*, Prentice-Hall, 1993.
[11] H.-Y. Fang, *Foundation Engineering Handbook*, Chapman & Hall, 1991.

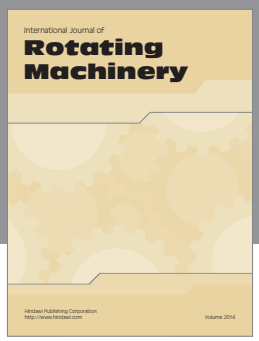

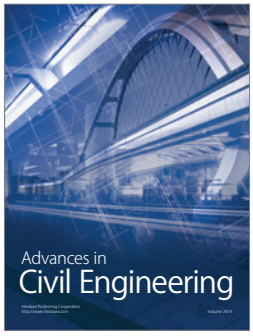

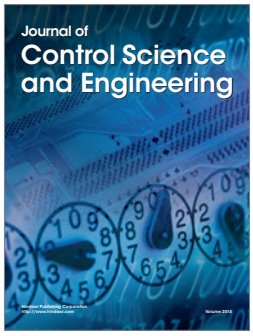

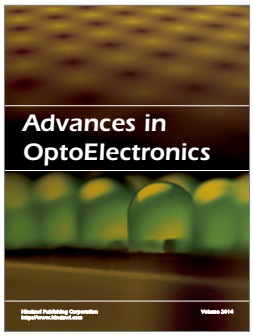

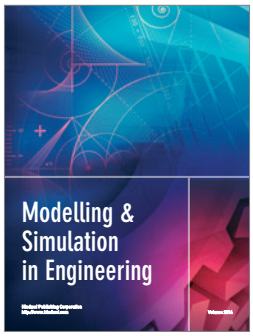

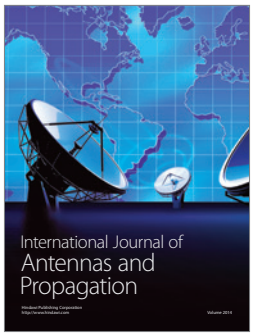

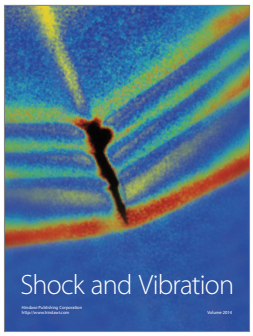

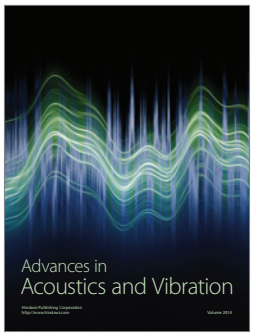

Hindawi

Submit your manuscripts at
http://www.hindawi.com